Atmos. Chem. Phys., 11, 3173–3194, 2011
www.atmos-chem-phys.net/11/3173/2011/
doi:10.5194/acp-11-3173-2011

Atmospheric Chemistry and Physics

Multi-scale modeling study of the source contributions to near-surface ozone and sulfur oxides levels over California during the ARCTAS-CARB period

M. Huang[1], G. R. Carmichael[1], S. N. Spak[1], B. Adhikary[1,2], S. Kulkarni[1], Y. Cheng[1], C. Wei[1], Y. Tang[3], A. D'Allura[4], P. O. Wennberg[5], G. L. Huey[6], J. E. Dibb[7], J. L. Jimenez[8], M. J. Cubison[8], A. J. Weinheimer[9], A. Kaduwela[10], C. Cai[10], M. Wong[11], R. Bradley Pierce[12], J. A. Al-Saadi[13], D. G. Streets[14], and Q. Zhang[14]

[1]Center for Global and Regional Environmental Research, University of Iowa, Iowa City, IA, USA
[2]School of Engineering, Kathmandu University, Dhulikhel, Nepal
[3]Meso-scale modeling, NOAA/NCEP/EMC, W/NP2, NOAA, Camp Springs, MD, USA
[4]ARIANET Srl, Milano, Italy
[5]Department of Environmental Science and Engineering and Division of Geological and Planetary Sciences, California Institute of Technology, Pasadena, CA, USA
[6]School of Earth & Atmospheric Sciences, Geogia Institute of Technology, Atlanta, GA, USA
[7]Institute for the Study of Earth, Oceans, and Space, University of New Hampshire, Durham, NH, USA
[8]Department of Chemistry, University of Colorado, Boulder, CO, USA
[9]NCAR, Boulder, CO, USA
[10]California Air Resource Board, Sacramento, CA, USA
[11]Department of Geography, The University of Maryland, College Park, MD, USA
[12]NOAA/NESDIS, Madison, WI, USA
[13]NASA Langley Research Center, Hampton, VA, USA
[14]Argonne National Laboratory, Argonne, IL, USA

Received: 22 October 2010 – Published in Atmos. Chem. Phys. Discuss.: 12 November 2010
Revised: 7 March 2011 – Accepted: 27 March 2011 – Published: 4 April 2011

Abstract. Chronic high surface ozone (O_3) levels and the increasing sulfur oxides ($SO_x = SO_2 + SO_4$) ambient concentrations over South Coast (SC) and other areas of California (CA) are affected by both local emissions and long-range transport. In this paper, multi-scale tracer, full-chemistry and adjoint simulations using the STEM atmospheric chemistry model are conducted to assess the contribution of local emission sourcesto SC O_3 and to evaluate the impacts of transported sulfur and local emissions on the SC sulfur budgetduring the ARCTAS-CARB experiment period in 2008. Sensitivity simulations quantify contributions of biogenic and fire emissions to SC O_3 levels. California biogenic and fire emissions contribute 3–4 ppb to near-surface O_3 over SC, with larger contributions to other regions in CA. During a long-range transport event from Asia starting from 22 June, high SO_x levels (up to ∼0.7 ppb of SO_2 and ∼1.3 ppb of SO_4) is observed above ∼6 km, but they did not affect CA surface air quality. The elevated SO_x observed at 1–4 km is estimated to enhance surface SO_x over SC by ∼0.25 ppb (upper limit) on ∼24 June. The near-surface SO_x levels over SC during the flight week are attributed mostly to local emissions. Two anthropogenic SO_x emission inventories (EIs) from the California Air Resources Board (CARB) and the US Environmental Protection Agency (EPA) are compared and applied in 60 km and 12 km chemical transport simulations, and the results are compared withobservations. The CARB EI shows improvements over the National Emission Inventory (NEI) by EPA, but generally underestimates surface SC SO_x by about a factor of two. Adjoint sensitivity analysis indicated that SO_2 levels at 00:00 UTC (17:00 local time) at six SC surface sites were influenced by previous day maritime emissions over the ocean, the terrestrial emissions over nearby urban areas, and by transported SO_2 from the north through both terrestrial and maritime areas. Overall maritime emissions contribute

Correspondence to: M. Huang
(mhuang1@engineering.uiowa.edu)

Published by Copernicus Publications on behalf of the European Geosciences Union.

10–70% of SO_2 and 20–60% fine SO_4 on-shore and over the most terrestrial areas, with contributions decreasing with inland distance from the coast. Maritime emissions also modify the photochemical environment, shifting O_3 production over coastal SC to more VOC-limited conditions. These suggest an important role for shipping emission controls in reducing fine particle and O_3 concentrations in SC.

1 Introduction

In the past 20 years, California population has increased by 33% and the economy has grown rapidly (Cox et al., 2009). In the meanwhile, California has taken good efforts to reduce the emissions of most primary pollutants and the entire state has met the state and national standards for most of these pollutants except tropospheric ozone (O_3) and particulate matter (PM). Nearly all Californians live in areas that are designated as nonattainment for the state (about 99%) and national (about 93%) health-based O_3 and/or PM standards.

O_3 is an atmospheric pollutant harmful to human health and agriculture, and is also one of themost important short-lived green-house gases (GHG). The US National Ambient Air Quality Standard (NAAQS) for daily maximum 8-h average O_3 has recently been lowered to 75 ppb, and is likely to be lowered further to between 60 ppb and 70 ppb in future regulatory reviews of its direct impacts on human health. The California Air Resource Board (CARB) currently sets more stringent state 1-h and 8-h O_3 standards at 90 ppb and 70 ppb to better address longstanding urban and regional O_3 problems. Despite the continued precursoremission reductions, limited improvement in O_3 has been achieved over the last decade. Local production from both natural and anthropogenic emission sources, together with inter-continental and in-state transport contributes to the O_3 levels over both urban and rural areas.

Aerosols play an important role in the climate system causing both direct and indirect effects (IPCC report, 2007). They can be transported thousands of kilometers due to their lifetimes of about a week, and adversely affect human health and visibility. Sulfate (SO_4) is an important component of ambient aerosols, and it hasa cooling effect on climate. Sulfur compounds emitted into the atmosphere are ultimately oxidized into SO_4, by a variety of oxidants such as hydroxyl radical (OH) and hydrogen peroxide (H_2O_2) in gas and/or liquid phases. Among various sulfur compounds, SO_2 remains an important primary atmospheric pollutant. It is a highly reactive gas harmful to human respiratory system. It can be emitted from both anthropogenic and natural sources, and can be produced from oxidation of other chemicals such as hydrogen sulfide (H_2S) by OH. SO_2 emissions from anthropogenic sources are generally thought to be better known than other species such as non-methane volatile organic compounds (NMVOCs). The documented largest sources of SO_2 emissions in the US are from fossil fuel combustion at power plants (66%) and other industrial facilities (29%) (US EPA, http://www.epa.gov/air/sulfurdioxide/). Various techniques have been used to control SO_2 emissions from these large sources. However, the major SO_2 emission sources over California vary with location. Unlike the continuous decreasing trend in statewide NO_x, VOC, and CO emissions through the past decades, anthropogenic SO_x emissions started to increase from 2005 and this trend is estimated to continue for the next 10 years. This increasing trend is mainly due to the emissions from the "other mobiles" categories, including the significant growth in shipping activities and the high-sulfur fuels that ocean-going vessels typically use, especially around the coastal areas such as San Francisco (SF) and Los Angeles (LA) counties (Cox et al., 2009). Although shipping emission control regulations are in action since 2009, the SO_2 levels over some South Coast (SC) surface sites are still increasing. In addition, SO_2 emitted from terrestrial industrial processes, certain modes of surface transport, and area sources contribute to the SO_x concentrations over southern California. Similar as for O_3 and its precursors, the long-range transport of SO_4 affects the California sulfur budget. Because of various health concerns, the US EPA has recently tightened the primary standard for 1-h SO_2 to 75 ppb and changed the SO_2 monitoring requirements. The design of effective emission reduction strategies requires estimates of the factors that influence the regional background pollution levels and the local enhancements. A number of observational and modeling studies have been conducted to quantify the effects of sector emissions on near-surface O_3 and SO_x levels. It has been concluded that less than 40 ppb of O_3 are contributed by natural sources (Fiore et al., 2003; Wang et al., 2009; Koo et al., 2010). As for anthropogenic emissions, the effects of shipping emissions on regional air quality have been shown important since 1997 (Corbett et al., 1997) over different regions. For example, Vutukuru et al. (2008) focused their studies on the emissions from the LA – Long Beach area, where one third of the cargo containers to the US arrive (BST associates, 2007). They estimated the impacts of shipping emissions on surface 1-h and 8-h O_3 to be up to >20 ppb, and the SO_2 emissions from shipping to cause a rise inon-shore SO_2 concentrations by 2–4 ppb in 2002, and is projected to grow to 8–10 ppb by 2020.

However, the accuracy of observational-based studies of estimating natural O_3 levels relies on the representativeness of measurement sites and the methods to filter out the local anthropogenic contributions (Fiore et al., 2003), and the studies of fire impacts on O_3 are mostly conducted by comparing O_3 levels during fire and non-fire periods, in which way daily variations due to other factors cannot be completely excluded (Viswanathanet al., 2006; Bytnerowicz et al., 2010). Model-based estimations are also uncertain as they are highly dependent on model resolutions, key inputs (such as emission inventories (EIs) andmeteorology conditions), chemical mechanisms, and the study periods (Pfister et al., 2008; Wang et

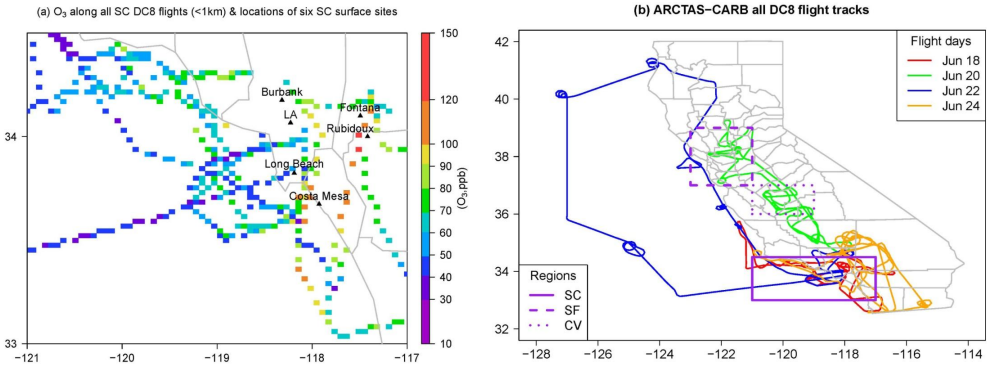

Fig. 1. (a) Observed O_3 along all SC flight path below 1 km, the locations of six SC surface sites are overlaid; **(b)** DC-8 flight paths on 18, 20, 22, 24 June during ARCTAS-CARB period, and the defined study regions.

al., 2009; Koo et al., 2010). Many of these modeling studiesuse coarse grids (from 36 km to several degrees horizontally), and the O_3 enhancement resulting from biogenic and fire sources are estimated either by tracer calculations (Pfister et al., 2008), or from simulations using purely natural emissions (Koo et al., 2010).

As one of the most important model inputs that affect the uncertainties of source contribution studies, EIs have been developed based on various data sources and assumptions, with different spatial and temporal variability. Their reliability needs to be validated. A previous field experiment, the Intercontinental Transport and Chemical Transformation of Anthropogenic Pollution (ITCT), conducted by NOAA in 2002 discovered the potential underestimation in sulfur species emissions (2010 CalNex science and implementation plan, 2008). The uncertainties imported from EIs in source contribution studies need to be quantified. By using two natural EIs (SMOKE and MEGAN), natural O_3 backgrounds differed by 4 ppb in a 2002 study and were close in a 2018 case (Koo et al., 2010). Model simulations with different EIs and the comparisons with various three-dimensional observational datasets are important methods to complement the EI validation and provide better understanding of uncertainties of source contribution studies.

In this paper we estimate various source contributions to the regional background O_3 levels and local enhancements of SO_x by analyzing observations obtained during the California portion of the Arctic Research of the Composition of the Troposphere from Aircraft and Satellites (ARCTAS-CARB) field experiment period (18–24 June 2008) using the STEM regional-scale modeling system. The system used includes tracer andfull-chemistry models at two different spatial and temporal resolutions. Based on the modeled pollutant spatial patterns and the quantity of flight observational data, we mainly focus this study on California's South Coast (SC) region. We look at the near-surface O_3 and SO_x distributions over SC (and other regions) and identify the effects of long-range transport and local contributions. The long-range transport of SO_x during a specific period is discussed in this paper (O_3 transport during this period was discussed in Huang et al. (2010)). We quantify the effects of the local emissions from natural sources (i.e., biogenic and wildfires) on O_3 levels with two different EIs in two resolutions, and estimate the impacts of maritime emissions on on-shore air quality in the finer grids. We also compare results using two SO_x EIs with observations and identify areas where further improvements are needed. Adjoint sensitivities are calculated and used to study the impacts of daytime and nighttime terrestrial and maritime SO_2 emissions on surface SC SO_2 levels.

2 Methods

2.1 Mission and source data

The ARCTAS-CARB field experiment was conducted in June 2008 by the National Aeronautics and Space Administration (NASA). The NASA DC-8 aircraft platform sampled trace gas and aerosol concentrations through four scientific flights over California on 18, 20, 22 and 24 June 2008 and the flight paths are shown together in Fig. 1b. Three (18, 22, 24 June) out of the four flights took measurements over the SC area during the daytime (∼15:00–24:00 UTC (08:00–17:00 local time)). This mission had multiple scientific objectives, including improving the state emission inventories, characterizing off-shore shipping emissions, and quantifying the import of pollution from Asia (Jacob et al., 2010). Ozone was measured by the NCAR team using the Chemiluminescence method. Two SO_2 measurement teams (CIT and GIT) and two SO_4 measurement teams (UNH and CU – Boulder) were on board for all the flights. (http://www-air.larc.nasa.gov/cgi-bin/arcstat-c). The CIT and GIT teams both used chemical ionization mass spectroscopy (CIMS), and UNH and CU-Boulder (CUB) used Soluble Acidic Gases and Aerosol (SAGA) and Aerosol Mass Spectrometry (AMS), respectively (Weinheimer et al., 1994; Scheuer et al., 2003;

McNaughton et al., 2007; Slusher et al., 2004; Crounse et al., 2009; Dunlea et al, 2009). These data were averaged every one minute for use in this study.

We focus this study on the SC area because it had the largest number of flight-collected air samples, although analysis was also done over the SF and the Central Valley (CV) area. The SC, SF and CV domains are defined in boxes in Fig. 1b. The latitude/longitude ranges that the three regions cover are 33° N–34.5° N, 121° W–117° W; 37° N–39° N, 123° W–121° W; 36° N–37° N, 119° W–121° W, respectively.

In addition to the airborne measurements, surface measurements were analyzed. The data analyzed included continuous hourly SO_2 measurements with low instrument sensitivity and hourly O_3 concentrations from six CARB surface sites. The locations of these sites are shown in Fig. 1a and more detailed descriptions are provided in the supplementary material (http://www.arb.ca.gov/qaweb/siteinfo.php). Sulfate aersol data used included: EPA Air Quality System (AQS) daily-averaged fine PM (diameter 0–2.5 µm) speciation data (including SO_4) at a variety of California urban sites on 20 and 23 June (http://www.epa.gov/ttn/airs/airsaqs/detaildata/downloadaqsdata.htm, referred as "STN" in this paper); daily-averaged fine SO_4 mass from Interagency Monitoring of Protected Visual Environments (IMPROVE) sites on 20 and 23 June (http://views.cira.colostate.edu/web/DataWizard/); and weekly-averaged SO_4 mass at six Californian Clean Air Status and Trends Network (CASTNET) surface sites over the remote areas (http://java.epa.gov/castnet/index.jsp). Several CASTNET and IMPROVE sites are co-located.

2.2 Model, meteorology and boundary conditions

We simulated the ARCTAS – CARB period (18–24 June) usingthe Sulfur Transport and dEposition Model (STEM) – Version 2K3. The modeling system applied here included three components: (1) a hemisphere tracer model in 60 km polar stereographic grids (http://www.cgrer.uiowa.edu/ARCTAS/arctas-2k8.html); (2) a continental scale gasphase and aerosol chemical transport simulation in 60 km grids on a subset of (1) (http://www.cgrer.uiowa.edu/ARCTAS2/arctas2-2k8.html), and (3) a regional-scale gasphase and aerosol chemical transport domain centered over California in a 12 km Lambert conformal conic grid, covering Nevada and part of Mexico. The SAPRC-99 chemical mechanism was used (Carter, 2000). This mechanism has been applied to many US cases and compared with several other mechanisms (Chen et al., 2010; Luecken et al., 2008). Meteorology fields for all three grids were generated by the Advanced Research Weather Research & Forecasting Model (WRF-ARW) Version 2.2.1 (Skamarock et al., 2007) with forecast and reanalyzed meteorological inputs (Mesinger et al., 2006) for the 60 km and 12 km simulations, respectively. Different boundary conditions were used in this study for the 60 km and 12 km simulations. In the 60 km base case, lateral boundary conditions (LBC) for thirty gaseous species and top boundary conditions for ten gaseous species were obtained from the archived RAQMS global model predictions. The LBCs for BC, OC, dust, sea salt and SO_4 were taken from the 60 km STEM tracer results. Boundary conditions for the 12 km simulations came from the 60 km full-chemistry simulations. The details of the model configuration are described in Huang et al. (2010) and in Table 1.

We also used the adjoint of STEM (Sandu et al., 2005; Chai et al., 2009) to study the SO_2 sensitivity with respect to receptor (the SC surface sites in this case) SO_2 concentration during the flight week (Sect. 3.7) in the 12 km regional simulation. This adjoint approach has been applied in previous studies for source attribution and for data assimilation (Carmichael et al., 2008). Model forward sensitivity studies quantify the change of chemical distributions in all grids at future times in response to the perturbation of model inputs. In contrast, adjoint sensitivities represent backward in time the change of chemical distributions in those grids that influence a given receptor at a specific time.

2.3 Emissions

Emission inputs for each of the three modeling components differed slightly, based on respective demands for resolution and completeness. In the hemispheric tracer model, we used a bottom-up global gridded inventory developed forthe ARCTAS mission (developed by David Streets, Qiang Zhang et al., received in 2008, http://mic.greenresource.cn/arctas_premission). This inventory is driven by regional-specific information on fuels and activity from various economic sectors, and includes anthropogenic, biomass and global shipping contributions. In the 60 km continental model, anthropogenic emissions for North America were taken from the 2001 National Emissions Estimate Version 3 (NEI 2001), an update of the 1999 US National Emissions Inventory with growth factors applied by Source Classification Code, and augmented with national inventories for Canada (2000) and Mexico (1999). The NEI 2001 includes emission around the port area, but misses the shipping emissions over the open ocean. Daily biomass burning emissions from the Real-time Air Quality Modeling System (RAQMS) (Pierce et al., 2007) were provided by the Cooperative Institute for Meteorological Satellite Studies (CIMSS). Biogenic emissions of monoterpene and isoprene were taken from twelve-year-averaged values from the Orchidee model (Lathiere et al., 2006). For the 12 km model the anthropogenic and biogenic emissions were re-gridded from a contemporary CARB 4 km emission inventory. The anthropogenic emissions outside of the CARB domain (including Mexico, states of Nevada, Washington and Idaho) were taken from NEI 2001, same as in the 60 km base simulation. Biomass burning emissionswere generated by the prep-chem-source model (WRF/Chem Version 3.1 users' guide, 2009), which used

Table 1. Summary of STEM model inputs for base cases in two resolutions.

Inputs	Source Data		Resolutions	
	60 km/18 layers/6 h base case	12 km/32 layers/1 h base case	60 km	12 km
Meteorology, WRF 2.2.1	GFS + one time step SST	NARR + daily SST	6 h, 1°×1°	3 h, 36 km
Ozone column, required by the TUV model	Measured by Ozone Mapping Spectrometer (OMI) instrument on board the NASA Aura spacecraft, daily		1°×1°, 1 day	
Anthropogenic Emissions (point and mobile)	NEI 2001, weekday varied from weekends	CARB 2005, projected from 2002, daily varied. Out of CARB domain filled with NEI 2001	1°×1°, 1 h	4 km ×4 km, 1 h
Biogenic Emissions	Orchidee	CARB 2005 projected from 2002, daily varied	1°×1°, monthly averaged	4 km ×4 km, 1 h
Biomass burning Emissions	RAQMS real time	MODIS-detected hot spots, processed by prep-chem-source model; mass-conserved normalization	1°×1°, 12 h	1 km ×1 km, 24 h
Top and Lateral Boundary Conditions	RAQMS real time (gases) + STEM tracer (several aerosols)	STEM 60 km base case	2°×2°, 6 h and 60 km×60 km, 6 h	60 km ×60 km, 18 layers, 6 h

Acronyms:
GFS: Global Forecast System
NARR: North American Regional Reanalysis
MODIS: Moderate Resolution Imaging Spectroradiometer
TUV: Tropospheric Ultraviolet and Visible (TUV) Radiation Model
Other acronyms are defined in text.

MODIS – detected point fire information at 1 km ground resolution (Giglio et al., 2003; Davies et al., 2009) and was adjusted at each time step to match total emissions rates from RAQMS. H_2S and dimethyl sulfide (DMS) emissions were not included in these cases.

3 Results and discussions

3.1 General conditions and O_3 levels in base cases

The California summer climate in 2008 was hot and dry, influenced by the Pacific high pressure system. Wildfire events broke out on 21 June at various locations over both northern and southern California. On 18–20 June, fires were detected along the California-Mexico border.

The 12 km average WRF-modeled 10 m winds at multiple times (00:00, 06:00, 12:00 and 18:00 UTC – 17:00, 23:00, 05:00, 11:00 local time, respectively) over California during the experiment week are shown in Fig. 2. The northwesterly winds along the coast and through the Central Valley, together with the sea-land breezes, determined the regional transport of pollutants during this period. The wind vectors are overlaid on the WRF-predicted mixing layer height (PBLHT). The PBLHT over the ocean stayed below ∼600 m, while the PBLHT over parts of the SC terrestrial areas reached up to ∼1500 m during daytime. These are consistent with the vertical structures of short-lived chemicals observed by the aircraft measurements (shown in Fig. 7, to be discussed).

The observed O_3 concentrations along all DC8 flights (Sect 2.1 and Fig. 1) below 1000 m are shown in Fig. 1a and 3e horizontally and vertically, respectively. Observed O_3 ranged from less than 40 ppb to ∼120 ppb with large variability. The highest O_3 levels (>120 ppb) were found around Riverside. The O_3 levels over the ocean were typically below 80 ppb.

The modeled O_3 concentrations from the 12 km simulations are shown in Fig. 3a and b, for the 15:00–24:00 UTC-averaged O_3, and for the daily averaged maximum O_3, respectively. The predicted O_3 concentrations over the Central Valley and southern California are over 70 ppb during the flight times. The averaged O_3 levels during the flight times over northern California, southern California urban areas are 5–10 ppb lower. The predicted average daily maximum O_3 levels occur in the Central Valley and a large part of southern California (>90 ppb).

Finer grid simulations are usually expected to better capture local features. However, coarser grids (in this study, the 60 km) simulations (typically used in global models and in forecast-mode regional model simulations) with different model inputs are also valuable to evaluate the uncertainties of model sensitivity to sector emissions, which will be described in detail in Sect. 3.2. The base case simulations are shown in this section first. The modeled O_3 concentrations from the 60 km simulations are presented in Fig. 3c and d, for the averaged 15:00–24:00 UTC O_3, and for the averaged daily maximum O_3, respectively. Overall the 60 km simulations show similar spatial patterns over CA compared with the 12 km results, but lower O_3 concentrations over the Central Valley and southern California.

Figure 3e compares the predicted $O_3$for the two model resolutions with all flight observations below 1000 m vertically. The 12 km simulations captured the observed variability fairly well, with the correlation of 0.62. It generally overpredicted the O_3 concentrations, but captured the higher observed concentrations (>75% quantile, mostly over terrestrial regions) better, with mean bias 11.6 ppb and root mean square error 13.9 ppb. The 60 km simulations showed less

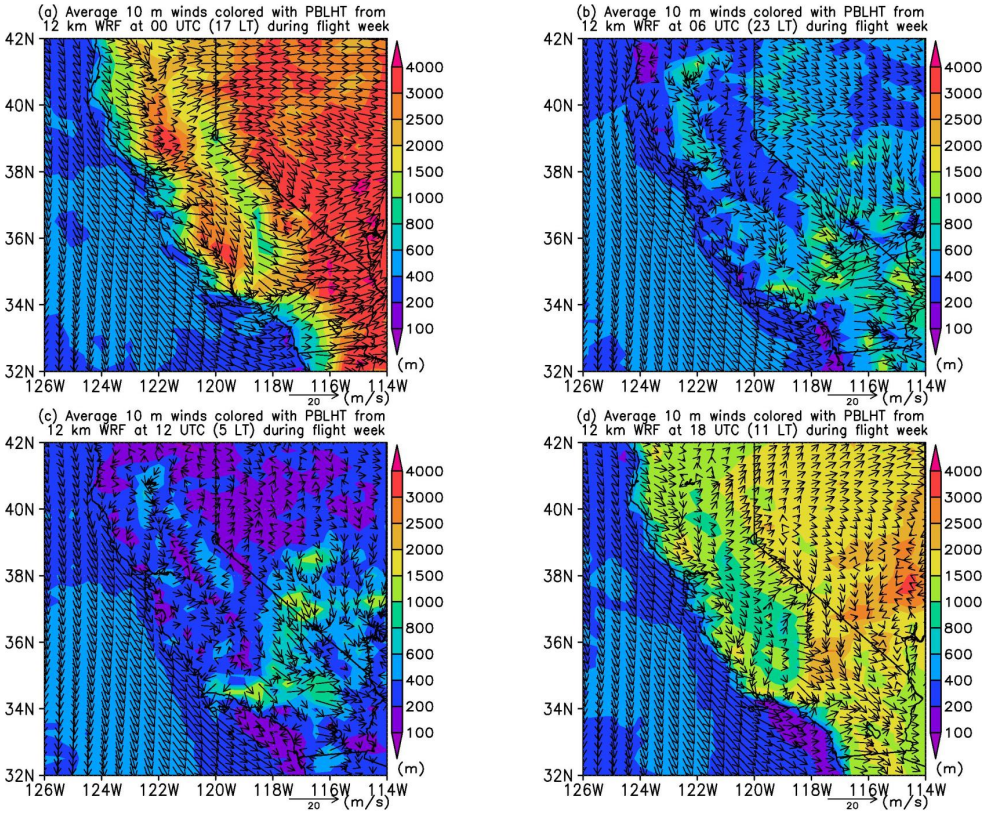

Fig. 2. Weekly-average 12 km WRF 10 m wind fields, at **(a)** 00:00 UTC (17:00 local time) **(b)** 06:00 UTC (23:00 local time) **(c)** 12:00 UTC (05:00 local time) **(d)** 18:00 UTC (11:00 local time), overlaid on 12 km WRF-predicted mixing layer height (m).

vertical variability, but similar correlation with observations ($r = 0.58$) as the 12 km simulations. Its extent of overprediction of O_3 was lower than the 12 km case, but the simulations for the higher-observed concentrations (>75% quantile) showed higher biases, with mean bias of 15.9 ppb and root mean square error of 19.8 ppb.

Figure 3f compares the observed and modeled O_3 time series averaged over the six CARB surface sites (Fig. 1a) during the flight week. No significant weekday-weekend variations (21 and 22 June are Sat. and Sun.) are found. The 12 km simulation results were well correlatedwith the observations ($r = 0.73$), and captured the daytime variations fairly well. Nighttime O_3 concentrations were over-predicted by 10–30 ppb, due to the under prediction of nighttime NO_x and uncertainties in the transport of upwind O_3 concentrations. The 60 km results showed lower correlations ($r = 0.6$) and weaker diurnal variations, with higher overpredictions during the night time. It is harder for the coarser grids to capture the night time titration processes and the transport of background O_3 from the upwind locations.

3.2 Influences of natural source emissions on SC O_3

In order to quantify the impacts of natural emission sources on SC O_3 levels, we conducted two sensitivity simulations in the 12 km grids. We turned off the biogenic (isoprene and monoterpene) emissions and wildfire emissions for the two cases, respectively, and analyzed the changes of O_3 between the base and each of the sensitivity cases.

Figure 4a shows the 24-h average isoprene and monoterpene emissions from the CARB EI. Their emissions are highly related to the land use type (not shown) and vary over California. Isoprene and monoterpene emission rates are the highest over northern California regions covered by evergreens, and account for 40–60% of total NMVOC emissions over those regions. In contrast, in the Central Valley and south coast urban areas, the emission rates are more than 20 times lower, accounting for less than 2% of the total NMVOC emissions (not shown).

The differences of flight time (15:00–24:00 UTC) and daily maximum surface O_3 concentrations during the flight week between the base and no-biogenic emission cases are shown in Fig. 4c, and e, respectively. The largest O_3 decreasesis found over northern California and the CV, with the flight time O_3 changes up to 6 ppb and the average daily maximum changes from 6 to12 ppb. In contrast, the O_3 changes over the SC area are shown smaller, between 2 and 4 ppb.

The impacts of fires on 24-h average surface CO during the flight week are shown in Fig. 4b. The highest differences

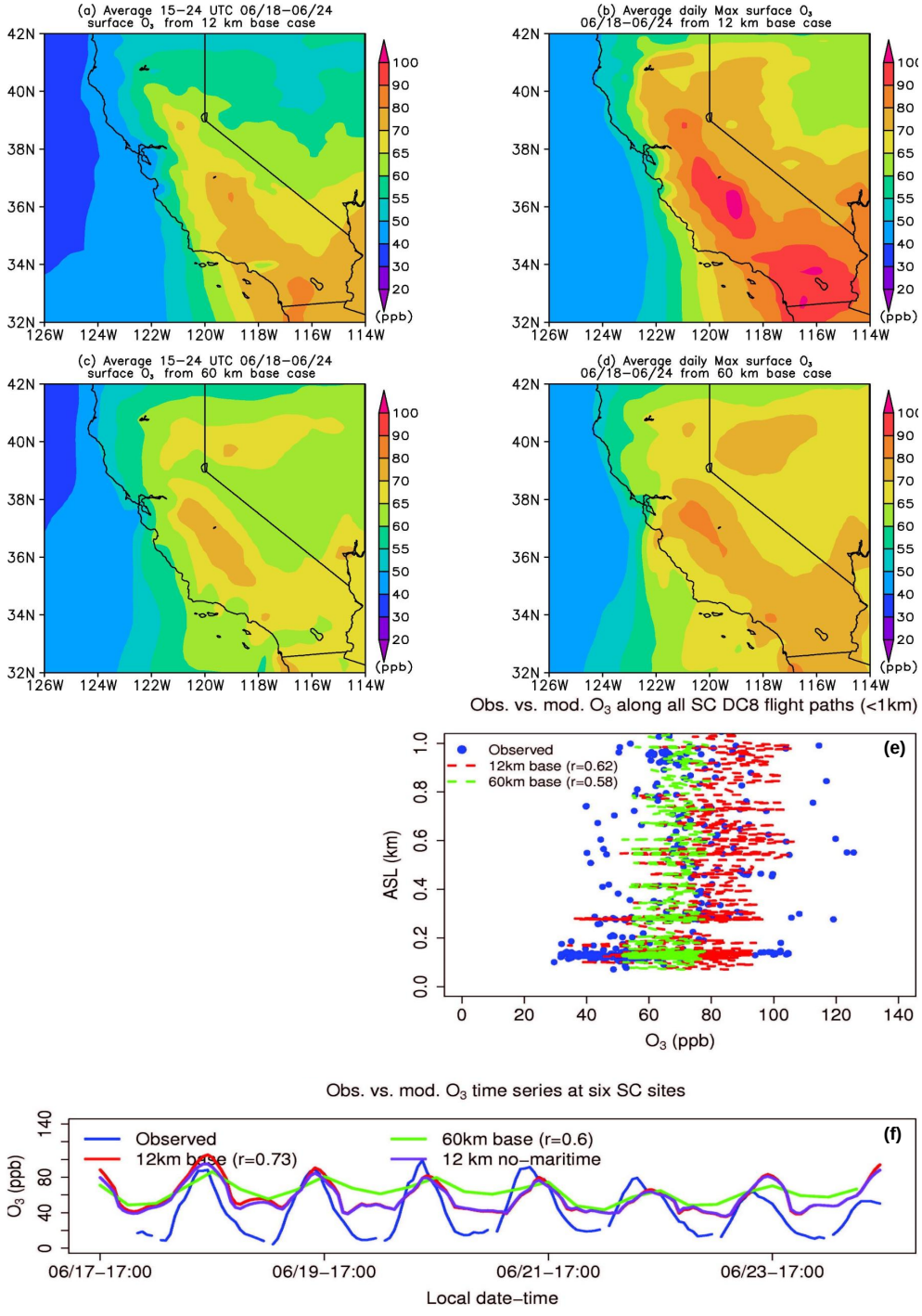

Fig. 3. (a–b) 12 km and **(c–d)** 60 km modeled **(a, c)** average 15:00–24:00 UTC (08:00–17:00 local time) and **(b, d)** daily maximum surface O_3; **(e)** Observed and modeled O_3 vertical profiles along all SC flight paths below 1 km; **(f)** Observed and modeled (60 km base, 12 km base and no-maritime emissions cases) O_3 time series at six SC surface sites.

(>100 ppb) due to California fires occur over northern California, where the wildfires were most intense and durations the longest. Fire locations with changes in CO of 400–800 ppb are shown in northern California and the Monterey Bay areas, and the fire impacts on CO extend to the SC coastal areas (20–50 ppb of delta CO between base and no-fire cases). Analysis of the impacts from wildfires in North Asia and Europe, and South Asia and Africa using the tracer model indicate that the fires thatoccurred outside of the North America had negligible impacts on surface SC air quality

Table 2. Modeled O_3 sensitivity along flight paths below 1 km from both resolution cases.

12 km			Biogenic			Fire
Flight day	Mean (%)	Max (%)	Number of points with sensitivity >10%/total number of points (%)	Mean (%)	Max (%)	Number of points with sensitivity >10%/total number of points (%)
18 June SC	1.36	4.98	0	0.28	0.65	0
20 June SC	/	/	/	/	/	/
22 June SC	1.64	3.73	0	2.81	13.72	5
24 June SC	5.04	8.87	0	14.47	26.55	62.50
all SC	2.3	8.87	0	4.26	26.55	16.14
all CA	2.84	19.87	1.98	4.78	30.2	19.85
60 km			Biogenic			Fire
Flight day	Mean (%)	Max (%)	Number of points with sensitivity >10%/total number of points (%)	Mean (%)	Max (%)	Number of points with sensitivity >10%/total number of points (%)
18 June SC	6.04	26.5	15.7	3.19	25.65	5.38
20 June SC	/	/	/	/	/	/
22 June SC	1.63	5.57	0	2.05	6.2	0
24 June SC	1.48	3.92	0	5.43	17.04	15.38
all SC	3.8	26.5	7.85	3.41	25.65	6.28
all CA	5	26.78	9	5.34	26.1	13

(<5% below ∼1.5 km, not shown) during this period. The differences of flight time (15:00–24:00 UTC) and daily maximum surface O_3 during the flight week between the base and no-fire emission cases are shown in Fig. 4d and f, respectively. The largest changes in averaged daily maximum O_3 occur over the northern part of the California-Nevada border (9–15 ppb). Negative O_3 changes can be found around the fire locations, indicating the strong influences of aerosol emissions from fires. Over the SC area, the fire impacts on the average surface maximum and flight time O_3 are ∼1–3 ppb.

To better understand the impact of biogenic and fire emissions on O_3 concentrations within the boundary layer, we calculated the model sensitivity for each of the one-minute flight data below 1000 m, using Eq. (1).

$$\text{Sensitivity (\%)} = \frac{|\text{base case } O_3 - \text{sensitivity case } O_3|}{\text{base case } O_3} \times 100\% \quad (1)$$

The model sensitivities are plotted in Fig. 5a and b. The sensitivities in both cases are below ∼30%, O_3 over the CV area was largely affected by biogenic emissions. The O_3 levels over northern CV, the SF coast, and the central coast were highly impacted by the fire emissions.

The mean and maximum sensitivity for each flight day in SC are summarized in Table 2. The mean 12 km model results show that biogenic and fire emissions contributed 2.3% and 4.3%, respectively, to near surface O_3 over SC (with maximum values reaching contributions of 8.9% and 26.6% for each of these sources, respectively). The contributions of biogenic and fire emissions were higher in regions outside of SC.

To help assess the uncertainties in estimating the role of natural emissions, no-biogenic and no-fire emission sensitivity simulations were also conducted in the 60 km grid domain. The 24-h average Orchidee EI (Fig. 6a) shows a smoother but similar spatial pattern as the 12 km CARB estimates, with the maximum emission rates over northern California, lower than the CARB EI. Moreover, the magnitudes are much lower than the CARB EI along the coastal areas and higher over southeastern California. Delta O_3 between the 60 km base and no-biogenic emission cases are shown in Fig. 6c and e. The changes in average daily maximum O_3 are of similar magnitude as in the 12 km grids over northern California and CV, but are 5–8 ppb over the SC area, higher than the changes in the 12 km grids. The O_3 changes during flight times (15:00–24:00 UTC) also differ from the 12 km cases, with higher magnitudes overall (changes over the SC of 5–6 ppb). The different O_3 changes over SC between the two resolution cases are not only due to the emission differences within California, but also reflect the impacts of model resolution on flow fields, mixing layer height, and the contributions from the Nevada and Mexico biogenic emissions,which the CARB EI does not include.

The differences of daily maximum surface O_3 during the flight week between the base and no-fire emission cases in 60 km grids are shown in Fig. 6f. Same as in the 12 km cases, the highest changes occur over the north part of California-Nevada border (9–15 ppb). Figure 6d shows higher flight time average O_3 changes than in the 12 km cases (approximately doubled magnitudes over most areas). Negative O_3 changes are not found over California because the coarse resolution smooths the intensity of fire emissions, as the CO

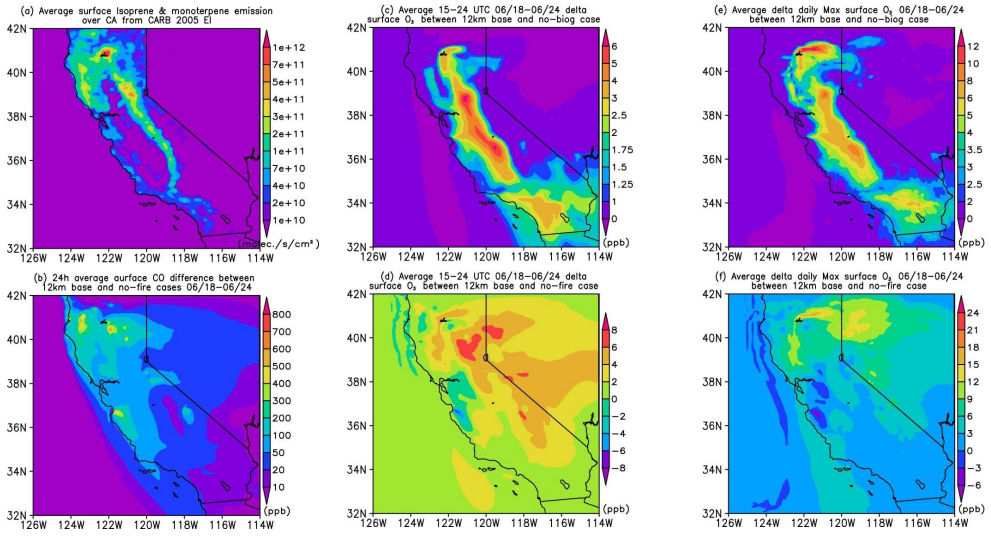

Fig. 4. (a) Average surface isoprene and monoterpene emissions from CARB EI **(b)** 24 h-average differences of CO between base and no-fire cases in 12 km grids; Surface O_3 differences between **(c, e)** base and no-biogenic cases and **(d, f)** base and no-fire cases of **(c–d)** averaged 15:00–24:00 UTC (08:00–17:00 local time) and **(e–f)** average daily maximum O_3 in 12 km grids.

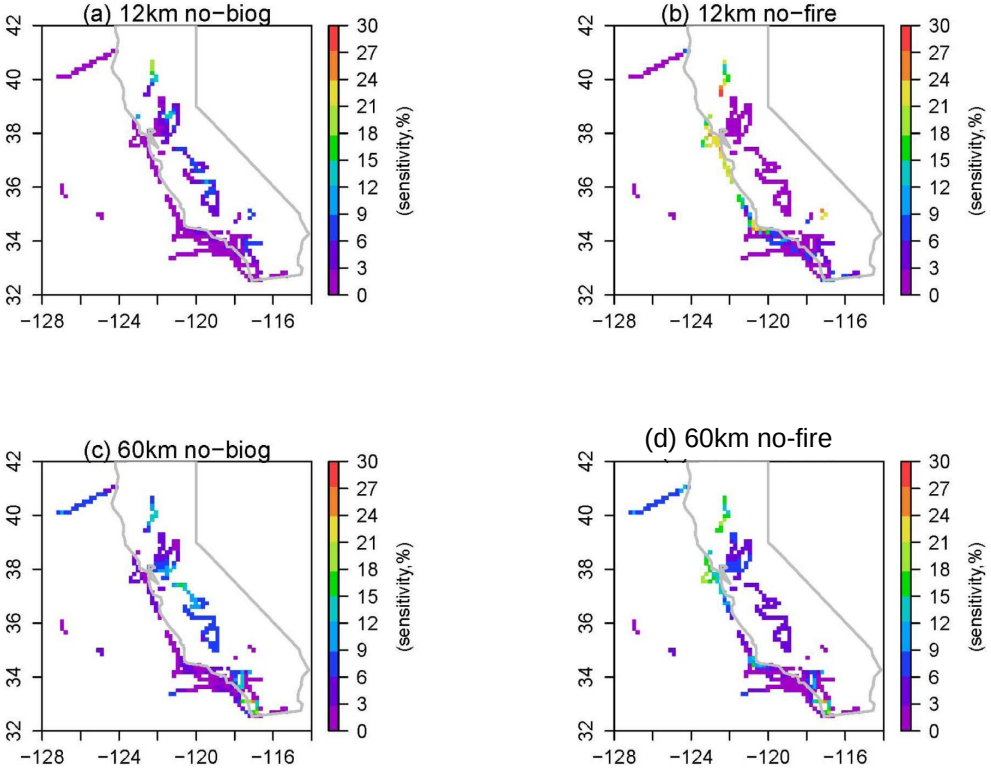

Fig. 5. Model O_3 sensitivity for **(a, c)** no-biogenic case **(b, d)** no-fire case from the 12 km **(a–b)** and 60 km **(c–d)** cases.

differences in Fig. 6b show. Over the SC area, the fire impacts on the average surface maximum and flight time O_3 are less than ∼4 ppb.

The model sensitivity along all SC flight paths below 1000 m in 60 km grids are shown in Fig. 5c, d and Table 2. The 60 km simulations show high sensitivity of O_3 to biogenic emissions along the southern California-Mexico border. Due to the Mexico biogenic emissions, the 60 km differences between base and no-biogenic emissions cases are higher at SC. Stronger model sensitivity to fire emissions is found over that

region and less strong sensitivity to fire emissions can be seen along the coastal SC areas, indicating the effects of model resolution and fire locations.

The sensitivity studies conducted in two resolutions suggest that fire and biogenic emissions play more important roles in O_3 production over areas outside of SC during the ARCTAS-CARB period. The different model configurations indicate a 3–4 ppb uncertainty due to various factors (such as resolution, EIs, emission injection heights, meteorology fields).

3.3 SO_x spatial distributions and model-observation comparisons

Observed and modeled SO_x spatial-temporal distributions over SC are discussed in this section. The 60 km domain was used in forecast mode in support of the ARCTAS experiment. The evaluation of the 60 km results found significant negative biases. This motivated the 12 km simulations designed in the post-analysis stage to assess the impacts of model resolution, EI and other factors on model prediction skills.

The model-predicted 24-h surface average total sulfur levels during the experiment week from the 12 km and 60 km simulationsare shown in Fig. 7a and c. The corresponding SO_2 contributions to total sulfur (SO_2+SO_4, SO_4 was converted to ppb) are also shown in Fig. 7b, d. Elevated sulfur levels can be seen over SC, SF and Fresno in CV, as well as around the California – Nevada border and the west California – Mexico border, due to the fresh emissions (SO_2% >60%). The sulfur levels at these areas from the 60 km simulations are generally lower than the 12 km case, especially over the SC area. Due to the lack of the shipping emissions in the NEI 2001, the sulfur levels over the ocean are low in the 60 km case, except the near-shore areas of the central coast. In contrast, the 12 km base case shows more detailed local features over land and the gradients along ship tracks in the ocean.

Figure 7e and f shows the observed total sulfur along all DC-8 flights (below 1 km a.s.l.), together with the SO_2% in the SC area. The observed total sulfur is the sum of averaged SO_2 and SO_4 (units are converted to ppb) measured by different teams. The SO_2% is the ratio of the averaged SO_2 concentrations measured by the two teams over the total sulfur concentrations. Similar to the model simulations, fresh SO_2 (SO_2% >60%) and higher sulfur levels were observed within the SC domain. Over SC, SO_x levels were higher at on-shore port areas, such as around Long Beach (up to 5–12 ppb), than over the inland areas (below ∼0.5–2 ppb).

The modeled total sulfur concentrations are compared with observations along all SC DC-8 flights (below 5 km a.s.l.), and are shown as vertical profiles in Fig. 7i. The steps used to combine the data from different measurement teams to create average observed values are described here. First, we calculated SO_2 and SO_4 profiles separately. As there were two SO_2 and two SO_4measurements by different institutional teams,if there are two measurements at any location along the flight paths, we used the average. If there was only one measurement, we used it directly. If there was no data, we treated it as missing value. We then calculated SO_x =SO_2 + SO_4. For locations with no SO_2 or SO_4 data, we treated it as missing value. The vertical structures constructed by binning data every 500 m and averaging them, show that sulfurwas enhanced from the surface to ∼3–4 km. The observed average surface sulfur over this region was ∼1.8 ppb below 500 m. The predictions show the lowest sulfur (and the highest biases) in the 60 km base case. The 12 km base case also under-predicted total sulfur at all altitudes, but were improved over the 60 km base predictions.

Comparisons of observed and modeled SO_2 and SO_4 along all DC-8 flight paths over the three regions are shown as vertical profiles in Fig. 7g and h. The GIT SO_2 is lower than the CIT SO_2 below 1 km and higher at ∼1–3 km. The two sets of measured SO_4 follow the same trend below ∼1.5 km, but CU Boulder SO_4 is ∼10–20% lower than the UNH SO_4, and both teams observed SO_4 aloft at 2–4 km. The 60 km base case predicted the lowest SO_2 and SO_4. The 12 km base case SO_2 generally followed the CIT SO_2, but was biased low by ∼50% at the surface. The general vertical structure of SO_4 was captured, but was more than 50% under-predicted at most altitudes.

The comparisons of observed and modeled SO_2 and SO_4 along all DC-8 flight paths (at all altitudes) are summarized in Table 3. The R values between modeled and observed SO_x, the Mean Biases (MB) as well as Root Mean Square Error (RMSE) of modeled SO_2 and SO_4 are listed. The higher correlations and lower errors are in bold. The 60 km base case predicted lower SO_2 and SO_4, and showed the weaker correlations with the observations. The 12 km base case improved the modeled SO_2 and SO_4 in magnitudes and correlations. As the partitioning between SO_2 and SO_4 is highly dependent on OH we also compared predicted OH and found that the 12 km base case had higher correlation than the 60 km case (0.47 compared to 0.41, respectively).

In addition to the comparisons of modeled SO_x along the DC-8 flight tracks, we also compare the predicted SO_2 and SO_4 with surfaces sites. Figure 8a shows the averaged 15:00–24:00 UTC (08:00–17:00 local time) SO_2 at the six SC surface sites (locations shown in Fig. 1a). The 60 km base case under-predicted SO_2 more than 10 times in general (60 km results were multiplied by 10 to be shown in figure). The 12 km base case under-predicts by a factor of two overall, but produce higher maximum, minimum (not shown) and mean SO_2 values than 60 km, and are closer to the observations.

Fine aerosol SO_4 (diameter 0–2.5 µm) mass was measured at multiple AQS (STN) ground sites over California on 20 and 23 June, and at IMPROVE sites on the same days. These sites represent the fine SO_4 distributions over urban and rural areas, respectively. In addition, the total SO_4 mass was measured and analyzed once a week at six California

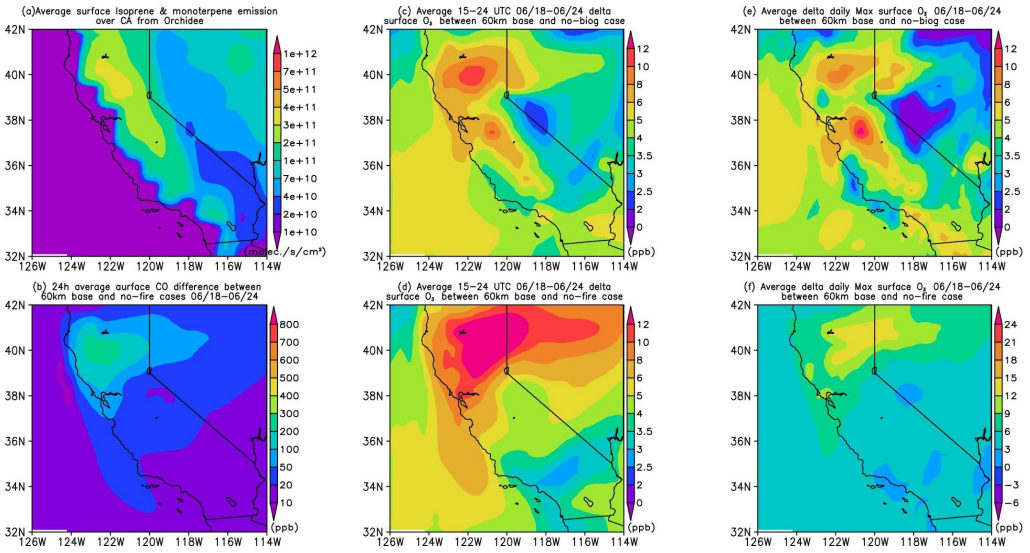

Fig. 6. (a) Average surface isoprene and monoterpene emissions from the Orchidee EI. **(b)** 24h-average differences of surface CO between base and no-fire cases in 60 km grids; Surface O_3 differences between **(c, e)** base and no-biogenic cases and (d, f) base and no-fire cases of **(c–d)** averaged 15:00–24:00 UTC (08:00–17:00 UTC) and **(e–f)** average daily maximum O_3 in 60 km grids.

Table 3. Correlation (R), Mean Biases (MB), Root Mean Square Error (RMSE) between modeled and observed SO_x along all SC flight tracks (all altitudes). Higher correlations, lower MB and RMSEs are in bold. Note that model comparisons refer to SC locations where measurements are available for individual teams, and the compared locations differ between teams.

Measurements	R (observations vs. predictions)		Observed Mean (ppb)	Mean Biases (ppb)		RMSE (ppb)	
	12 km Base	60 km Base		12 km Base	60 km Base	12 km Base	60 km Base
CIT SO_2	**0.36**	0.28	1.08	**0.41**	1.02	**1.55**	1.87
GIT SO_2	**0.43**	0.20	0.62	**0.13**	0.57	**0.81**	1.02
UNH SO_4	**0.54**	0.28	0.53	**0.30**	0.47	**0.39**	0.54
CUB SO_4	**0.50**	0.22	0.42	**0.22**	0.38	**0.40**	0.53

CASTNET sites, which are located at remote areas. Some CASTNET and IMPROVE sites are co-located. There are several AQS(STN) and IMPROVE sites located in SC domain, as Fig. 8b shows. No CASTNET sites are located in the SC domain (Fig. 8c).

These SO_4 observations are compared with results from both 12 km and 60 km simulations in Fig. 8b and c. The predictions from both cases are biased low by about a factor of two to three. The 12 km case results are improved over the 60 km predictions by more than a factor of two at the CASTNET and IMPROVE sites statewide and within SC, and slightly improved at STN sites.

From both modeled and observed SO_4 masses, it is found that during the flight week the surface values varied spatially according to: urban (AQS-STN) > rural and remote (IMPROVE CASTNET) areas, and both SC urban and rural areas had higher fine SO_4 than the statewide average.

Table 4. Ratios of observed and the 12 km simulated SO_x.

	(flight time) all SC flight observed/12 km predicted	(24 h) surface observed/ 12 km predicted
SO_2	1.71	1.35 (SC CARB) 1.79 for times 15:00–24:00 UTC
SO_4	2.48	2.56 (Statewide CASTNET)
Fine SO_4	3.17	2.5 (SC STN+IMPROVE)

In general, the 12 km results provide closer results to both flight and surface observations during the simulation week. We calculated the ratios of averaged observations over 12 km results along the flight paths and at surface sites in SC (Table 4). In general, the 12 km simulations underestimated SO_2 by up to ∼1.8 times and SO_4 by more than 2.5 times. During the flight periods, the ratios of the under-prediction along

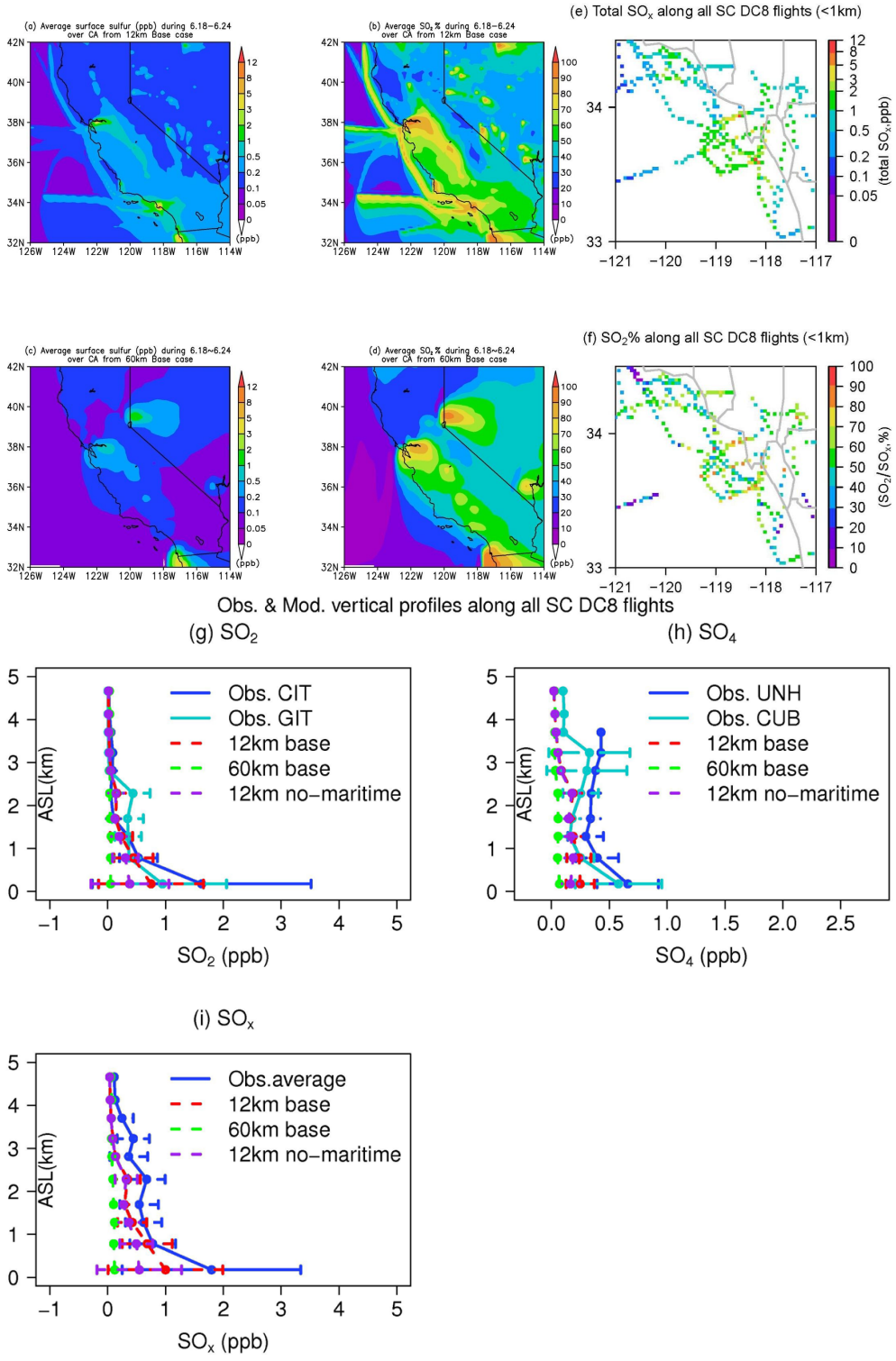

Fig. 7. The 24-h average surface **(a, c)** total SO_x and **(b, d)** SO_2% from 12 km **(a–b)** and 60 km **(c–d)** base simulations during the flight week; Observed **(e)** total SO_x and **(f)** SO_2% along all SC flights below 1 km. Observed and modeled **(g)** SO_2 **(h)** SO_4 and **(i)** SO_x vertical profiles along all SC flights (averaged every 500 m).

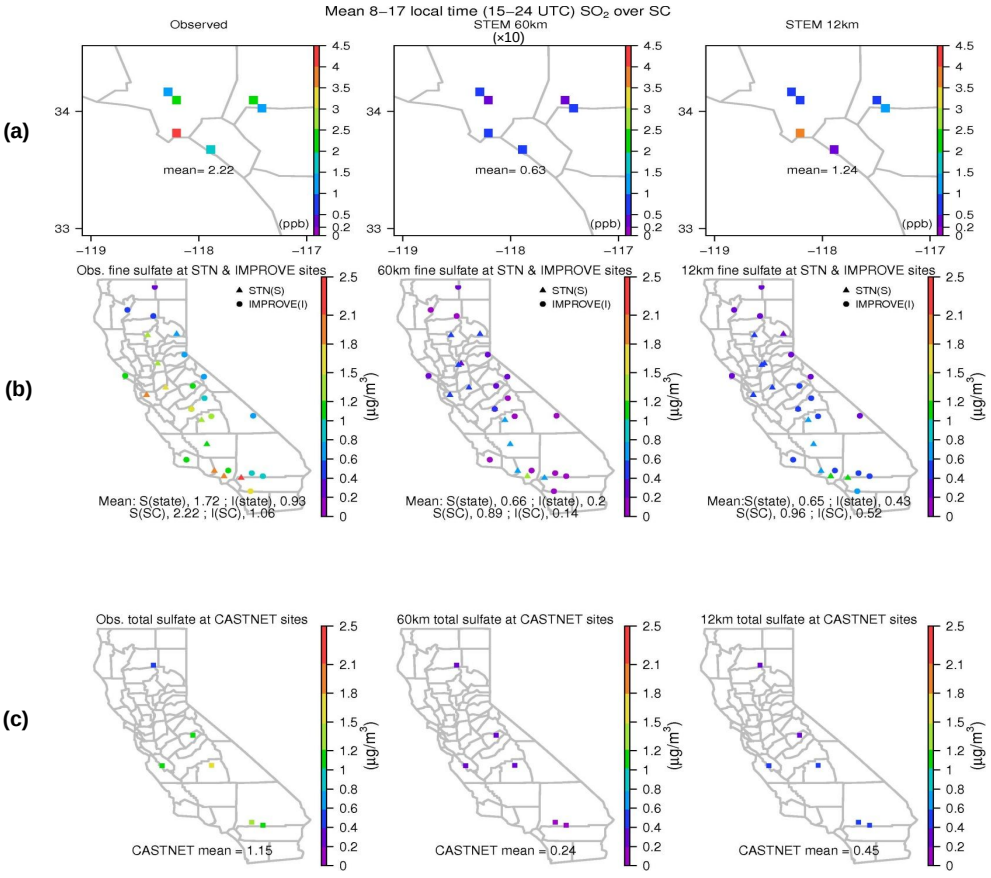

Fig. 8. (a) Observed and modeled average 15:00–24:00 UTC (08:00–17:00 local time) SO_2 at six SC surface sites; **(b)** Observed and modeled average fine SO_4 from STN and IMPROVE sites; **(c)** Observed and modeled average total SO_4 from six CASTNET sites during the flight week.

flight paths and at six surface sites were similar (1.71 and 1.79, respectively).

A similar analysis for SO_x was done over the SF and CV regions (Fig. 1b) and we suggest further improvement on EIs over these regions as well. In general, by using the CARB EI, the model underestimated SO_x concentrations by a factor of up to 2 in the SF region and more than 10 times around Fresno, and using NEI produced higher negative discrepancies. A more quantitative analysis of model biases for these regions was limited by the fact that many fewer flight observations were made over these regions during the experiment. In order to improve EIs over these regions, further studies are needed.

3.4 The identification of the contributors to the elevated SO_x concentrations

Figure 7g–i shows that SO_x was elevated along the SC flight tracks near surface and between 2–4 km. To better understand the possible source contributors to the elevated SO_x levels near the surface, we summarize the VOC age and CO contributions in Table 5 for flight segments below 1 km using the tracer calculations. VOC age was described in detail by Tang et al. (2004), which represents a combination of transport time, source intensities and diffusion, by using ethane as an indicator that is related to ethane emission and decay rate. During the experiment week, most of the flight-sampled airmasses had anthropogenic China CO% contributions less than 0.5% and North America CO% >99%, except the airmasses on 24 June during 23:00–24:00 UTC (during flight) that had China CO% of ∼40%. These airmasses are described in detail in Sect. 3.5.

In order to identify the airmass sources that caused the elevated sulfur aloft over SC between 2–4 km (Fig. 7g–i), we analyzed back-trajectories originating along the three SC DC-8 flight paths at 2–4 km a.s.l. on individual flight days, based on the 12 km meteorological fields. During the flights on 18 and 24 June, the air was lifted and moved from the Central Valley. In contrast, during the other flight day, airmasses were from the southwest, and they descended from >3500 m to SC (not shown in figures).

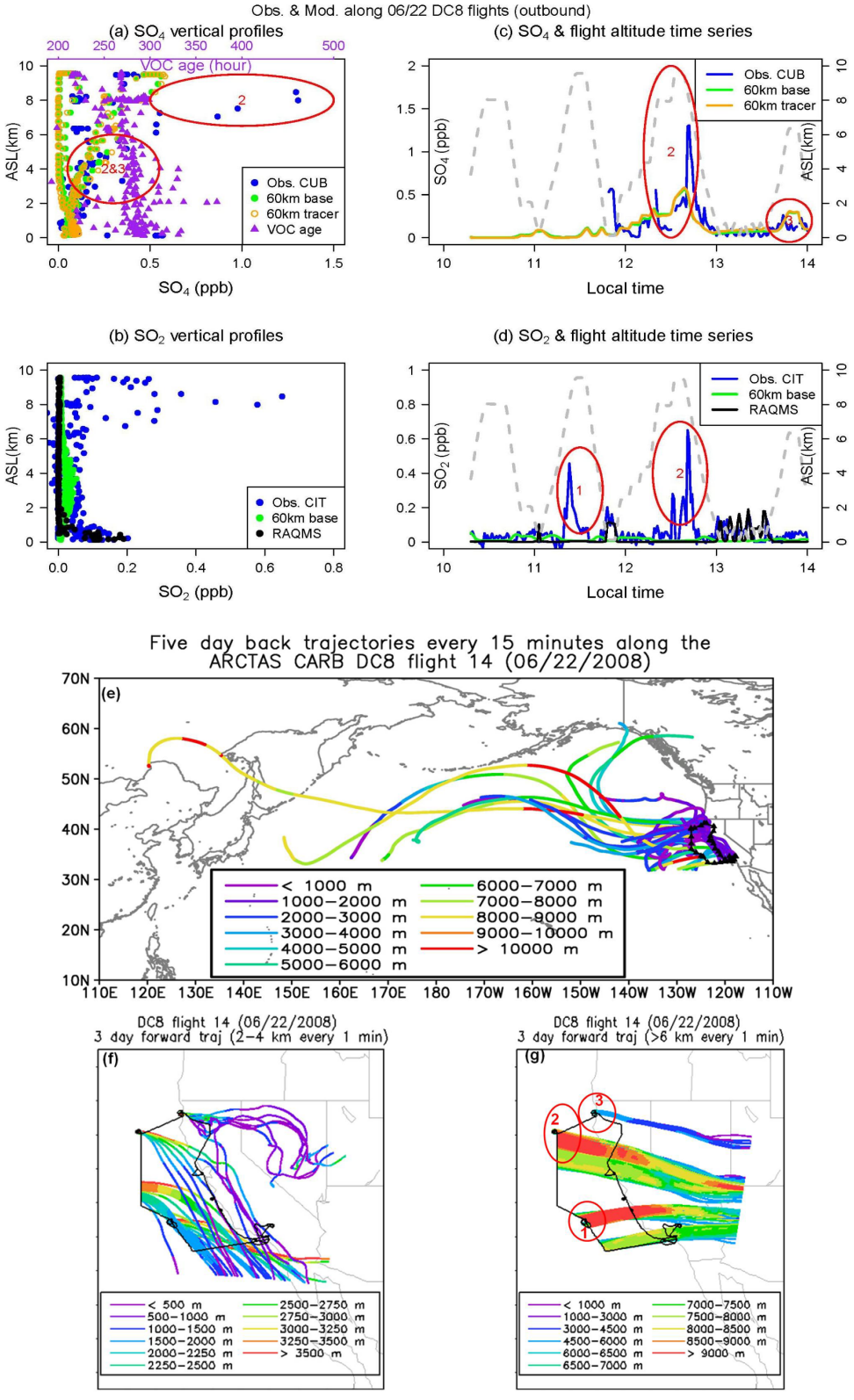

Fig. 9. Vertical profiles for (a) SO_4 (with tracer-calculated VOC age) and **(b)** SO_2 and time series (with flight altitudes) for **(c)** SO_4 and **(d)** SO_2 along outbound part of boundary layer flight on 22 June; **(e)** Back trajectories ending at the 22 June flight path **(f)** Three-day forward trajectories (a.s.l. 2–4 km) and **(g)** three-day forward trajectories (a.s.l. >6 km) starting from the outbound of the 22 June flight path.

Table 5. Air-mass properties below 1 km a.s.l. along three SC flight paths from observations and tracer calculations.

Flight day	VOC age (hour)	China CO (%)	North America CO (%)	SO_4-UNH (ppb)	SO_4-CUB (ppb)	SO_2-CIT (ppb)	SO_2-GIT (ppb)	SO_4 enhancements by foreign sources (ppb)	SO_2 enhancements by foreign sources (ppb)
18 June SC	11.26	0.01	99.94	0.6	0.44	1.31	0.87	3.1×10^{-4}	6.5×10^{-4}
22 June SC	10.73	0.2	99.74	0.55	0.56	1.37	/	1.4×10^{-3}	3.6×10^{-3}
24 June SC	15.78	16.61, (∼40% 23:00–24:00 UTC)	78.42, (∼40% 23:00–24:00 UTC)	0.63	0.58	/	0.55	0.13	0.12

3.5 Long-range transport events

Long-range transport of pollutants from Asia is typically assumed to be weaker and less frequent during summertime relative to springtime. During the ARCTAS-CARB experiment week, the 22 June flight aimed at characterizing the upwind boundary conditions necessary to model inland O_3 and aerosols (Jacob et al., 2010). On this day, the DC-8 took off from Palmdale, CA, flew over the Pacific Ocean to Trinidad Head (a northern California site shown suitable for studying airmass entering the western US), and then circled back to Palmdale along the coast (Fig. 1b). At the outbound part of this flight (approximating 17:00–21:00 UTC), strong Asian inflows were encountered, as indicated from the VOC age (ranging from 200–400 h) shown in Fig. 9a, together with the back trajectories based on the 60 km WRF meteorology fields in Fig. 9e. Vertical profiles and time series of observed and modeled SO_2 and SO_4 are shown in Fig. 9a–d for this flight. Red circles in figures match elevated SO_x concentrations in vertical profiles and time series plots to spatial locations shown in Fig. 9g. The 60 km tracer and 60 km full-chemistry simulated SO_4 are compared with the observations in Fig. 9a–b. (The LBCs used in the 60 km full-chemistry simulations were taken from the 60 km tracer SO_4 predictions and the 12 km full-chemistry simulations used LBCs from the 60 km full-chemistry results). Both the models captured the magnitudes of SO_4 at 2–4 km fairly well. Elevated SO_4 was also observed at 6–8 km a.s.l. (up to ∼1.3 ppb), mainly at location 2 and partially at location 3, by the CUB team. These airmasses were also high in China CO% based on the tracer model calculations at 6–8 km (Fig. 9a). Three-day forward trajectories originating from >6 km a.s.l. flight heights based on the 12 km WRF meteorology fields are shown in Fig. 9g, and the airmasses at these heights generally traveled above 3 km a.g.l. over California and thus did not impact the CA surface concentrations.

At flight location 3 (THD), the DC-8 also observed slightly enhanced SO_4 at 1–4 km (Fig. 9a). In a previous study, we concluded that elevated O_3 levels at 2–4 km on the same flight day in the eastern Pacific can be transported into the northern Central Valley, and contribute to the elevated surface O_3 at inland locations. These airmasses containing elevated SO_4 are also transported further into southern California (Fig. 9f). We estimate that these airmasses contributed ∼0.13 ppb to near-surface SO_4 levels over SC on 24 June, as summarized in Table 5. The upper limit enhancements of SO_4 by foreign airmasses along the SC flight paths are calculated by Eq. (2)

$$\text{Enhancements} = (1 - \text{North America CO\%}) \times \text{average } SO_x \text{ by two teams} \quad (2)$$

SO_2 peaks (<0.7 ppb) were also observed by the CIT team at 6–8 km a.s.l. at flight locations 1 and 2. These were the residuals in Asian plumes, as indicated by similar peaks for a number of observed species and the tracer calculations (not shown). The RAQMS and the 60 km base case results used as boundary conditions missed the SO_2 peaks at both locations 1 and 2, but as discussed for SO_4, these airmasses containing high SO_2 did not affect California surface air quality. Around 0.1 ppb of near-surface SO_2 was attributed to foreign sources (Table 5), and the boundary conditions captured SO_2 levels at 2–4 km very well (Fig. 9b).

3.6 SO_x local emissions – Emission Inventory comparisons

As the local emissions mainly contributed to the elevated SO_x concentrations near the surface during the experiment period, it is important to understand the contributions of the local sources. Therefore the emission inventory is one of the most important model inputs affecting the model-simulated near-surface SO_x concentrations.

Figure 10 compares the 24-h average surface SO_x emissions during 18–24 June from the CARB EI and NEI 2001 EI simulations (12 km and 60 km cases) over SC. Shipping emissions are included in the CARB EI,but are not in the NEI 2001, and the terrestrial SO_2 emissions in NEI 2001 are generally much lower as shown in Fig. 10 a and b. Figure 10c compares the time series of the average emission rates over the six SC surface sites from both EIs. The CARB EI peaks around noon time, while the NEI shows sharper later afternoon peaks (p.m. rush hours). The magnitudes in CARB emission rates are much higher than NEI, ∼12 times for the 24 h averaged emission rates at the six sites (6×10^{10} and 5×10^{9} molecules/cm^2/s, respectively).

Table 6 quantifies the mean and maximum surface SO_x emission rates in SC and the entire state from both EIs. The statewide mean and maximum emission rates from NEI are higher than the CARB EI. However, in SC, the situation is opposite. The largest SO_x emission sources in SC and California in NEI and CARB EI also differs. In the CARB EI,

Table 6. Maximum and mean SO_x emission rates over California and SC from both EIs and their top emissions sectors.

		Maximum (kg S/km^2/day)	Mean (kg S/km^2/day)	Top Emission Sector
CARB	Statewide	55.11	0.09	Ships and commercial boats, 52.1%
	SC	55.11	0.81 (regional total: 48.5 ton/day)	Ships and commercial boats, 44.6%
NEI	Statewide	173.14	0.13	Fossil fuel combustion, 51.3%
	SC	0.70	0.05 (regional total:4.91 ton/day)	Non-road equipment, 40.4%

– The sector emissions ranks in CARB and NEI documentations are for summertime South Coast Basin and yearly Los Angeles County, respectively, not the same as our SC domain, In their SC domain, CARB documented 2005 and 2010 summer SO_x emissions are 51.46 ton/day and 38.83 ton/day, respectively.
– Data sources: http://www.epa.gov/air/emissions/so2.htm, http://www.arb.ca.gov/app/emsinv/t25cat/cat_top25.php.

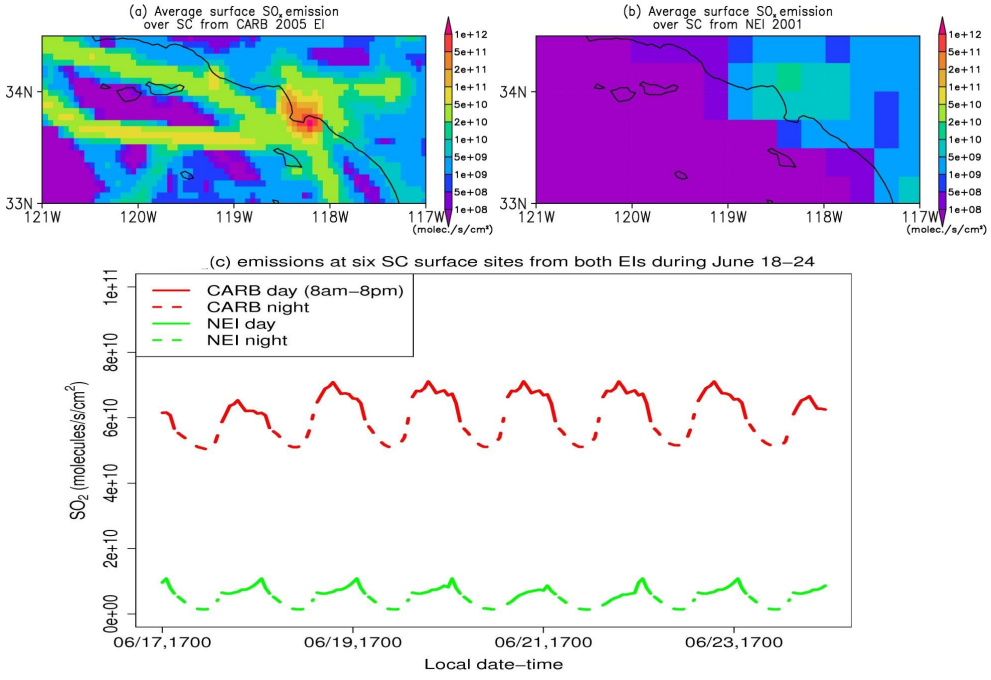

Fig. 10. The average surface SO_x (SO_2+Primary SO_4) during 18–24 June over SC from **(a)** CARB EI and **(b)** NEI 2001; **(c)** SO_x surface emissions from both EIs during 18–24 June over SC, solid and dash lines represent day (08:00–20:00 local time) and night time, respectively.

the shipping emissions account for 52.1% and 44.6% of summertime SO_x emissions for SC and the entire state, while in NEI, fossil fuel combustion and non-road equipment rank as the top emission sources in LA county and California, respectively. The regional total emissions from CARB EI (48.5 ton S/day) is ∼10 times of that documented by NEI (4.91 ton S/day).

3.7 Effects of maritime emissions on coastal SC air quality

As analyzed in Sect. 3.6, shipping emissions over the SC (and other California coastal areas) account for more than 40–50% of total summertime SO_x emissions. Therefore, the SO_x levels at SC are impacted by both terrestrial (highway, port heavy transportations, industry) and maritime emissions (mainly shipping). As for the important O_3 precursors, the maritime emissions account for ∼19% and 14.5% of the total NO_x emissions in SC and the state, while VOC emissions from ships are negligible.

In order to better understand the model SO_2 sensitivity with respect to SO_2 at receptor sites (the six SC surface sites shown in Fig. 1a), adjoint sensitivity simulations are conducted. Specifically we perturbed SO_2 concentrations at 00:00 UTC of each day during the flight weekand in the four surrounding model grids of all receptor sites. The influence function λ [SO_2] represents SO_2 sensitivity at earlier times in various locations in response to the perturbations in SO_2 at the receptors. The sensitivity runs for each day lasted for one day.

Figure 11a shows the weekly-averaged surface λ [SO_2] during the time periods (15:00–24:00 UTC), and Fig. 11c depicts the weekly-averaged λ [SO_2] vertical structures averaged over maritime and terrestrial grid cells during these

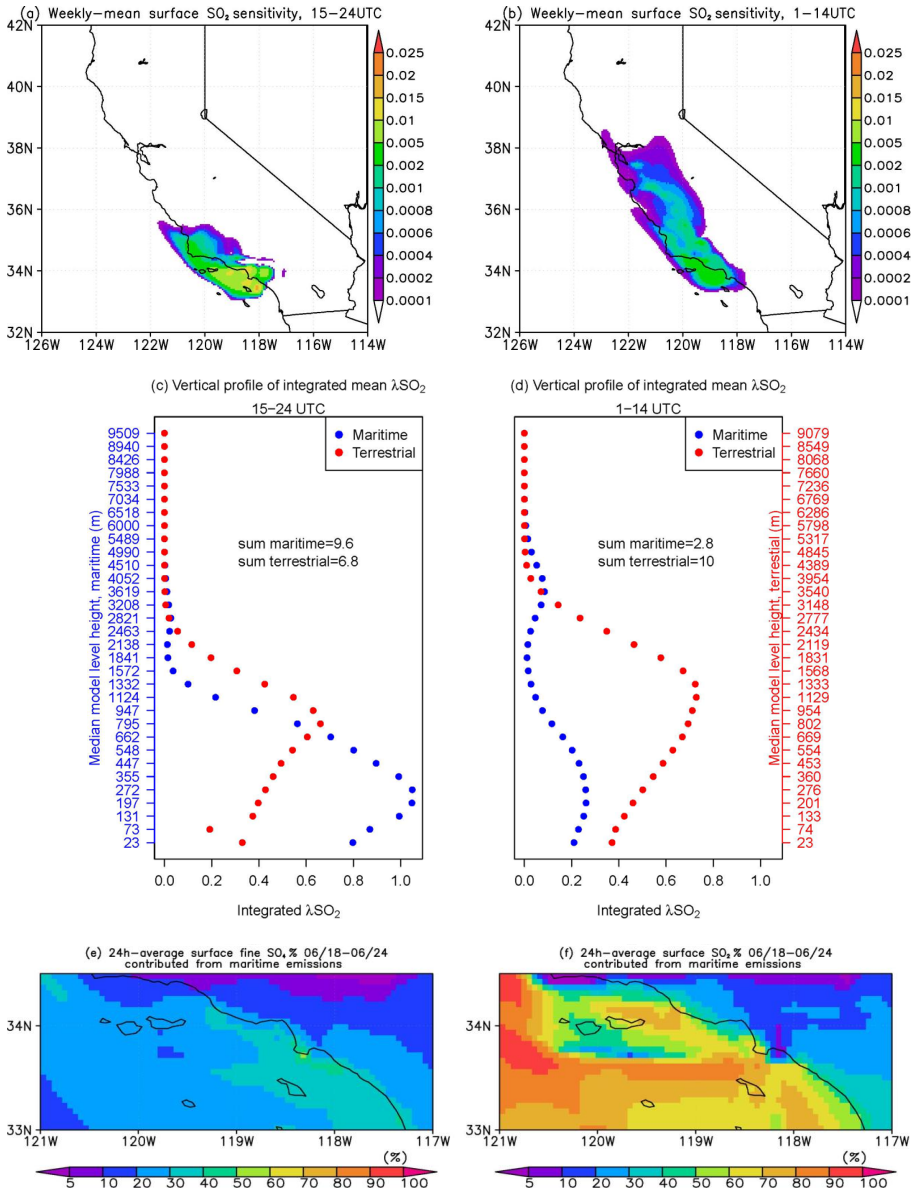

Fig. 11. Weekly mean surface SO_2 sensitivity for **(a)** 15:00–24:00 UTC **(b)** 01:00–14:00 UTC; Vertical profile of integrated mean SO_2 sensitivityfor **(c)** 15:00–24:00 UTC **(d)** 01:00–14:00 UTC; The 24-h averaged surface **(e)** SO_4% and **(f)** SO_2% contributed from maritime emissions over SC, calculated in 12 km grids.

times. SO_2 at the CARB monitoring site receptors is more sensitive to the maritime SO_2 levels than the terrestrial levels, especially over the surrounding areas of the ports and along the major shipping tracks, which reflect the impacts of the on-shore daytime transport associated with the sea breeze circulations during these periods. The vertical structures of λ [SO_2] reflect the modeled boundary layer structures over the land and ocean. The model level heights vary with location (for example, over the terrestrial regions, model level 10 ranges 730–860 m a.g.l. and over the oceanmodel level 5 is generally <300 m). Therefore, the integrated λ [SO_2] at each level are shown against the median model level height over the maritime and terrestrial regions.

Similarly, Fig. 11b shows the weekly-averaged surface λ [SO_2] during the rest of the times (at night and early morning, 01:00–14:00 UTC, 18:00–07:00 LT), after the peak in daytime boundary layer height. Figure 11d depicts the weekly-averaged maritime and terrestrial λ [SO_2] vertical structures for these times. At these times, SO_2 levels at the six SC sites are more sensitive to the terrestrial SO_2 levels than the maritime levels, and the sensitivities are generally lower than during the daytime (15:00–24:00 UTC times), with smaller

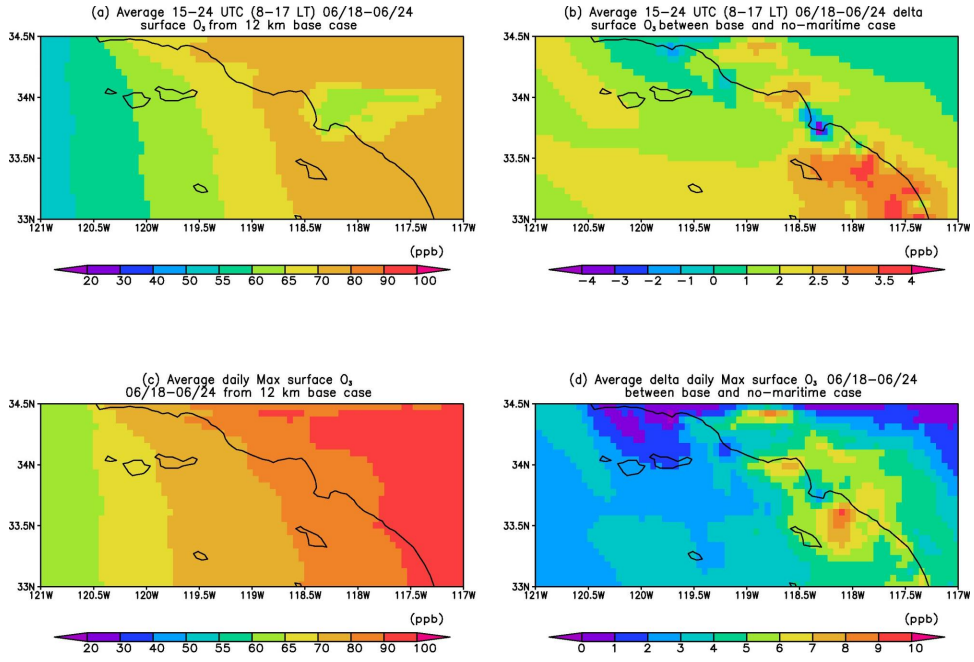

Fig. 12. (a) Averaged 15:00–24:00 UTC (08:00–17:00 local time) surface O_3 from 12 km base case; **(b)** Averaged 15:00–24:00 UTC (08:00–17:00 local time) surface O_3 differences between 12 km base and no-maritime emission cases; **(c)** Average daily maximum surface O_3 from 12 km base case; **(d)** Average daily maximum surface O_3 differences between 12 km base and no-maritime emission cases during the flight week.

gradients. The sensitivity regions are shown to extend to the San Francisco Bay area, indicating the effects of regional transport. The vertical structures of λ [SO_2] reflect the transport of SO_2 over the ocean during these times, which include the near-surface transport (<300 m), and transport at higher altitudes (∼3.5 km), the local contribution over the SC region, and the transport through terrestrial regions along the north and central coast areas. The maximum λ [SO_2] is found at altitudes <∼1.5 km a.g.l. over land during these times.

To further understand the contributions from terrestrial and maritime emissions to sulfur and O_3 concentrations over SC, we conducted an additional model simulation in the 12 km domain with only the terrestrial emissions from the CARB EI for all chemical species. The differences between the base case and the terrestrial-emission-only case provide an estimate of the contribution from maritime emissions.

Figure 11e and f illustrates the 24 h-average contributions of maritime emissions on surface SO_x concentrations during 15:00–24:00 UTC through the flight week. SO_2 levels are directly affected by both terrestrial and maritime emissions as shown. The maritime emissions cause high SO_2 levels over the ocean and on shore (where SO_2 > 60–70% of the total sulfur), with contributions to total SO_2 levels ranging from 10–70%. For SO_4, the spatial distribution is highly influenced by reaction rates and the wind fields. SC is heavily under the impact of northwest winds during the daytime in this period. Consequently, the maritime emissions generally contributed 20–60% of fine SO_4 along the coastaland inland areas, with the regions of influence extending as far as San Diego and the California – Mexico border area.

Figure 7g–i shows the change of the vertical distributions of SO_x in response to cutting off maritime emissions along all SC DC-8 flight paths. During the flight periods, both SO_2 and SO_4 were reduced in the vertical up to ∼1500 m. The maximum reduction of SO_x (by ∼50%) is shown at the lowest 500 m. The differences in simulated SO_2 in the 12 km base and terrestrial emission cases are ∼0.3–0.5 ppb for each day during the week at the six surface sites (not shown).

The effects of maritime emissions on surface O_3 levels are shown in Fig. 12. The average O_3 changes during 15:00–24:00 UTC for the flight week are below ∼4 ppb, and over the port areas (such as north Long Beach, the flight time average O_3 increases by 3–4 ppb after cutting off the maritime emissions. The averaged daily maximum O_3 decrease by 3–10 ppb in the domain, and the decreases around north Long Beach are lower (∼3–4 ppb). Figure 3f shows the time series of O_3 at the six SC surface sites from the no-maritime emission case, together with observations and 12 km and 60 km base O_3 values. The differences in simulated O_3 in the 12 km base and terrestrial emission cases are below 5 ppb, and the maximum changes occurred at afternoon peak time on 18 June.

To better understand the reduction of SC O_3 caused by maritime emissions, the changes of two O_3 production indicator species (NO_y and O_3/NO_y) are analyzed in Fig. 13. We first evaluate the model-predicted NO_y concentrations

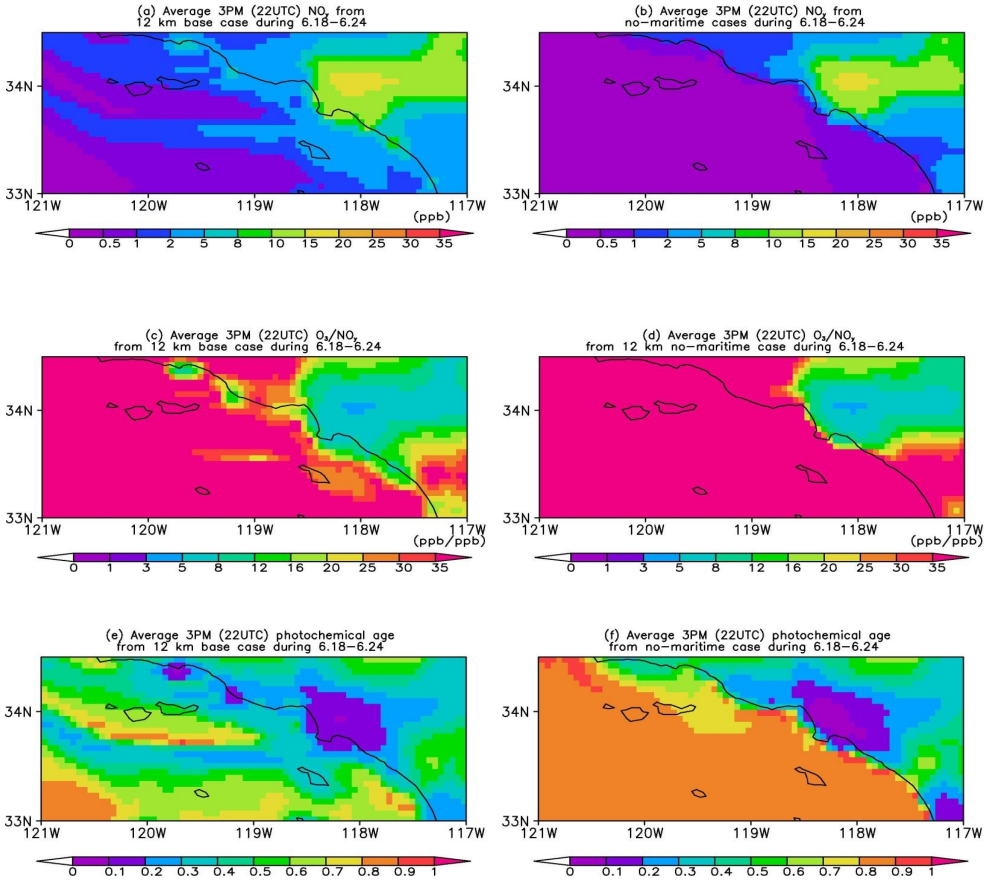

Fig. 13. **(a)** Average 22:00 UTC (15:00 local time) surface NO_y from **(a)** 12 km base case and **(b)** 12 km no-maritime case; **(c)** Average 22:00 UTC (15:00 local time) surface O_3/NO_y from 12 km base case and **(d)** 12 km no-maritime case; **(e)** Average 22:00 UTC (15:00 local time) surface photochemical age(NO_z/NO_y) from 12 km base case and **(f)** 12 km no-maritime case.

and O_3/NO_y ratios along all DC8 flights. Overall the model captured the main features of the spatial distributions for both of them, and the correlations of model predicted NO_y and O_3/NO_y (<0.5 km) were $R = 0.53$ and 0.71, respectively. The detailed validations of modeled O_3/NO_y and NO_y with flight observations are described in Huang et al. (2011).

Averaged NO_y and O_3/NO_y ratios at 15:00 (22:00 UTC) (the time of peak O_3 and PBL height) during the flight week are shown for the base and no-maritime emission cases. When afternoon NO_y <10–25 ppb, or/and O_3/NO_y >5–10, the area belongs to the NO_x-limited O_3 production regime (Milford et al., 1994; Sillman et al., 1995; Jacob et al., 1995). Based on these criteria, the SC urban area in the 12 km base case is estimated to be VOC limited. The removal of maritime emissions leads to flight time average NO_y decreases of up to >10 ppb, over the North Long Beach area, and the O_3/NO_y ratio rises up to 20 overthe regions south of Long Beach. This indicates that by cutting off the maritime emissions, some coastal areas can change from VOC-limited to NO_x-limited, or more NO_x-limited.

Photochemical age (PA) indicators such as NO_z/NO_y help us to evaluate the airmass smog potential. When PA is more than 0.6–0.7, smog potential is exhausted. Figure 13e and f show averaged at 15:00 (22:00 UTC) during the flight week for base and no-maritime emission cases. In both cases, PA are young (<0.6) over terrestrial areas, while the base case shows younger PA along shipping tracks (0.2–0.5), in contrast to PA in the no-maritime emission case (>0.8). Removing maritime emissions leads to old PA over most on-shore areas but slightly younger PA over SC urban areas.

4 Conclusions

The chronic high surface O_3 concentrations, as well as the increasing SO_x ambient concentrations over California's south coast (SC) and other regions, are affected by both long-range transport and local emissions, as shown in previous (Huang et al., 2010) and this study. Asian inflows were shown to be important around 22 June, during which period the O_3 concentrations in long-range transported air were 60–80 ppb. The transported air at ~2–4 km contained ~0.1–0.3 ppb of

SO_4 (Fig. 9a) in average. Those airmasses descended to the surface and influenced surface concentrations. The contribution from long-range transport occurred first over northern California and then over SC through in-state transport on ∼24 June, when up to ∼0.25 ppb of surface SO_x in SC was attributed to foreign sources (Table 5, upper-limit). During this period SO_4 and SO_2 in these long-range transported airmasses were also enhanced at altitudes above 6 km, but were transported at inland at high altitudes and did not influence CA surface air quality.

The influence of local emissions from both natural and anthropogenic sources on air quality was evaluated. We conducted sensitivity simulations by turning off biogenic and fire emissions in both 12 km and 60 km model resolutions and compared the modeled O_3 in base vs. sensitivity cases. We found that both biomass burning and biogenic emissions contribute to regional background O_3 over SC up to 4 ppb, with larger contributions in other regions of CA (such as in the Central Valley, up to 10–12 and 12–15 ppb from biogenic and fire emissions, respectively). Uncertainties in these estimates due to model resolutions, emissions inventories and other factors are on the order of 3–4 ppb over SC.

The high concentrations of SC surface SO_x during the flight week were mostly contributed by local emissions. We compared two anthropogenic SO_x EIs applied in 60 km and 12 km simulations and evaluated the model performance. The EIs vary temporally and spatially, but the NEI 2001 lacks the shipping emissions, and has lower emissions overall. The resulting predicted SO_x concentrations are shown to be significantly underestimated. The CARB 2005 EI improved the magnitudes of emission rates and produced results closer to observations. However, the overall SO_x emissions over the SC are found to be underestimated, and estimate that the CARB emissions are low by about factor of two.

Adjoint sensitivity analysis indicated that during the flight week, SO_2 levels at 00:00 UTC at six SC surface sites were influenced by previous day maritime emissions over the ocean, the terrestrial emissions over nearbyurban areas, and by transported SO_2 from the north, through both terrestrial and maritime areas.

We analyzed the effects of maritime emissions on air quality over SC by conducting a sensitivity simulation without maritime emissions using the CARB EI. The maritime emissions contributed 10–70% of SO_2 concentrationsover onshore and terrestrial areas, showing apparent negative gradients from the coastal to inland regions. Approximately 20–60% of fine SO_4 over the terrestrial regionsare attributed to the maritime emissions, and the impacts are extended to San Diego areas. The maritime emissions significantly increased the NO_y distributions on shore, especially around the port area of North Long Beach. The O_3 production in downwind areas can be shifted from VOC-limited to NO_x-limited after cutting off maritime emissions. Photochemical ages are also modified over on-shore areas as well as urban regions.

These results suggest that further improvements in SO_x emission inventories for the studied region as well as its upwind regions (north and central coastal areas) are needed. Optimal methods (such as data assimilation) can provide complete emission scaling factor matrix and reduce the mismatches between observations and model simulations. These methods would benefit from high resolution continuous near-surface measurements over both terrestrial and maritime areas. The impacts of one long-range transport event were analyzed during this one-week study period. Future studies over a longer period of time are needed to determine the frequency and variations in intensity of long range transport events and to identify the impacted regions during summertime. In addition, studies on reducing the uncertainties in estimated contributions from various emission sectors are also needed, which will support the future pollution control policies and regulations.

Supplement related to this article is available online at: http://www.atmos-chem-phys.net/11/3173/2011/acp-11-3173-2011-supplement.pdf.

Acknowledgements. We would like to thank the ARCTAS science team and two anonymous reviewers. We thank Tianfeng Chai (NOAA/OAR/ARL) for helping with the STEM adjoint model. This work was supported by a NASA award (NNX08AH56G). Jose L. Jimenez and Michael J. Cubisonwere supported by NASA NNX08AD39G. The authors would also like to acknowledge NOAA, the US EPA and CARB for support of the ground measurements. The views, opinions, and findings contained in this report are those of the author(s) and should not be construed as an official NOAA or US Government position, policy, or decision.

Edited by: P. Monks

References

BST Associates: Trade impacts studyPrepared for Port of Los Angeles, Port of Long Beach and Almeda Corridor Transportation Authority. http://www.portoflosangeles.org/DOC/REPORT_ACTA_Trade_Impact_Study.pdf, 2007.

Bytnerowicz, A., Cayan, D., Riggan, P., Schilling, S., Dawson, P., Tyree, M., Wolden, L., Tissell, R., and Preisler, H.: Analysis of the effects of combustion emissions and Santa Ana winds onambient ozone during the October 2007 southern California wildfires, Atmos. Environ., 44, 678–687, 2010.

Carmichael, G. R., Sandu, A., Chai, T., Daescu, D. N., Constantinescu, E. M., and Tang, Y.; Predicting air quality: Improvements through advanced methods to integrate modelsand measurements, J. Comp. Phys., 227, 3540–3571, doi:10.1016/j.jcp.2007.02.024, 2008.

Carter, W. P. L.: Implementation of the SAPRC-99 chemicalmechanism into the models-3 framework. Report to theUnited States Environmental Protection Agency, http://www.engr.ucr.edu/~carter/pubs/s99mod3.pdf, 2000.

Chai, T., Carmichael, G. R., Tang, Y., Sandu, A., Heckel, A., Richter, A., and Burrows, J. P.: Regional NO_2 emission inversion through four-dimensional variational approach using SCIAMACHY tropospheric column observations, Atmos. Environ., 43(32), 5046–5055, 2009

Chen, X. Ren, J. Mao, Z. Chen, W. H. Brune, B. Lefer, B. Rappenglück, J. Flynn, J. Olson and J. Crawford, A comparison of chemical mechanisms based on TRAMP-2006 field data, Atmos. Environ., 44, 4116–4125, 2010.

Corbett, J. J. and Fischbeck, P. S.: Emissions from ships, Science, 278, 823–824, 1997.

Cox, P., Delao, A., Komorniczak, A., and Weller, R.: The California almanac of emissions and air quality 2009 edition, http://www.arb.ca.gov/aqd/almanac/almanac09/almanac2009all.pdf, 2009.

Crounse, J. D., DeCarlo, P. F., Blake, D. R., Emmons, L. K., Campos, T. L., Apel, E. C., Clarke, A. D., Weinheimer, A. J., McCabe, D. C., Yokelson, R. J., Jimenez, J. L., and Wennberg, P. O.: Biomass burning and urban air pollution over the CentralMexican Plateau, Atmos. Chem. Phys., 9, 4929–4944, doi:10.5194/acp-9-4929-2009, 2009.

Davies, D. K., Ilavajhala, S., Wong, M. M., and Justice, C. O.: Fire Information for Resource Management System: Archiving and Distributing MODIS Active Fire Data. IEEE T. Geosci. Remote Sens., 47(1), 72–79, 2009.

Dunlea, E. J., DeCarlo, P. F., Aiken, A. C., Kimmel, J. R., Peltier, R. E., Weber, R. J., Tomlinson, J., Collins, D. R., Shinozuka, Y., McNaughton, C. S., Howell, S. G., Clarke, A. D., Emmons, L. K., Apel, E. C., Pfister, G. G., van Donkelaar, A., Martin, R. V., Millet, D. B., Heald, C. L., and Jimenez, J. L.: Evolution of Asian aerosols during transpacific transport in INTEX-B, Atmos. Chem. Phys., 9, 7257–7287, doi:10.5194/acp-9-7257-2009, 2009.

Fiore, A., Jacob, D. J., Liu, H., Yantosca, R. M., Fairlie, T. D., and Li, Q.: Variability in surface ozone background over the United States: Implications for air quality policy, J. Geophys. Res., 108(D24), 4787, doi:10.1029/2003JD003855, 2003.

Giglio, L., Descloitres, J., Justice, C. O., and Kaufman, Y. J.: An Enhanced Contextual Fire Detection Algorithm for MODIS, Remote Sens. Environ., 87, 273–282, 2003.

Huang, M., Carmichael, G. R., Adhikary, B., Spak, S. N., Kulkarni, S., Cheng, Y. F., Wei, C., Tang, Y., Parrish, D. D., Oltmans, S. J., D'Allura, A., Kaduwela, A., Cai, C., Weinheimer, A. J., Wong, M., Pierce, R. B., Al-Saadi, J. A., Streets, D. G., and Zhang, Q.: Impacts of transported background ozone on California air quality during the ARCTAS-CARB period – a multi-scale modeling study, Atmos. Chem. Phys., 10, 6947–6968, doi:10.5194/acp-10-6947-2010, 2010.

Huang, M., Carmichael, G. R., Kulkarni, S., Spak, S. N., Chai, T., Oltmans, S. J., Jaffe, D. A.,Streets, D. G., Kaduwela, A., Weinheimer, A. J., and Huey, G. L.: Source attribution at western U.S. coastal receptors and the impacts of coastal-inland transport of pollutants and local fires on surface air quality, J. Geophys. Res., under review, 2011.

IPCC: Contribution of Working Group I to the Fourth Assessment Report of the Intergovernmental Panel on Climate Change, Climate Change 2007: The Physical Science Basis, Cambridge, UK and New York, NY, USA, Cambridge University Press, 2007.

Jacob D. J., Horowitz L. W., Munger J. W., Heikes B. G., Dickerson R. R., Artz R. S., and Keene W. C.: Seasonal transition from NO_x to hydrocarbon-limited conditions for ozone production over the eastern United States in September, J. Geophys. Res., 100, 9315–9324, 1995.

Jacob, D. J., Crawford, J. H., Maring, H., Clarke, A. D., Dibb, J. E., Emmons, L. K., Ferrare, R. A., Hostetler, C. A., Russell, P. B., Singh, H. B., Thompson, A. M., Shaw, G. E., McCauley, E., Pederson, J. R., and Fisher, J. A.: The Arctic Research of the Compositionof the Troposphere from Aircraft and Satellites (ARCTAS)mission: design, execution, and first results, Atmos. Chem. Phys., 10, 5191–5212, doi:10.5194/acp-10-5191-2010, 2010.

Koo, B., Chien, C.-Y.,Tonnesen, G., Morris, R., Johnson, J. Sakulyanontvittaya, T., Piyachaturawat, P., and Yarwood, G.: Natural emissions for regional modeling of background ozone and particulatematter and impacts on emissions control strategies, Atmos. Environ., 44, 2372–2382, 2010.

Lathiere, J., Hauglustaine, D. A., Friend, A. D., De Noblet-Ducoudre, N., Viovy, N., and Folberth, G. A.: Impact of climate variability and land use changes on global biogenic volatile organic compound emissions, Atmos. Chem. Phys, 6, 2129–2146, 2006, doi:10.5194/acp-6-2129-2006, 2006.

Luecken, D. J., Phillips, S., Sarwar, G., and Jang, C.: Effects of using the CB05 vs. SAPRC99 vs. CB4 chemical mechanism on model predictions: Ozone and gas-phase photochemical precursorconcentrations, Atmos. Environ., 42, 5805–5820, 2008.

McNaughton, C. S., Thornhill, L., Clarke, A. D., Howell, S. G., Pinkerton, M., Anderson, B., Winstead, E., Hudgins, C., Maring, H., Dibb, J. E., and Scheuer, E.: Results from the DC-inlet characterization experiment (DICE): Airborne versus surfacesampling of mineral dust and sea salt aerosols, Aerosol Sci. Technol., 40, 136–159, 2007.

Mesingera, F., DiMego, G., Kalnay, E., Mitchell, K., Shafran, P. C., Ebisuzaki, W., Jovic, D., Woollen, J., Rogers, E., Berbery, E. H., Ek, M. B., Fan, Y., Grumbine, R., Higgins, W., Li, H., Lin, Y., Manikin, G., Parrish, D., and Shi, W.: North American Regional Reanalysis. B. Am. Meteorol. Soc., 87(3), 343–360, doi:10.1175/BAMS-87-3-343, 2006.

Milford, J. B., Gao, D., Sillman, S., Blossey, P., and Russell, A. G.: Total reactive nitrogen (NO_y) as an indicator of the sensitivity of ozone to reductions in hydrocarbon and NO_x emissions, J. Geophys. Res., 99, 3533–3542, 1994.

NASA: OMI O_3 column data source: ftp://toms.gsfc.nasa.gov/pub/omi/data/ozone/Y2008/, 2008.

NCEP/NOAA: Real-time, global, sea surface temperature (RTG_SST) analysis data source: ftp://polar.ncep.noaa.gov/pub/history/sst/, 2008.

NOAA: 2010 CalNex Science and Implementation Plan, http://www.esrl.noaa.gov/csd/calnex/scienceplan.pdf, 2008

Pfister, G. G., Wiedinmyer, C., and Emmons, L. K.: Impacts of the fall 2007 Californiawildfires on surface ozone: Integrating local observations withglobal model simulations, Geophys. Res. Lett., 35, L19814, doi:10.1029/2008GL034747, 2008.

Sandu, A., Daescu, D. N., Carmichael, G. R., and Chai, T.:Adjoint sensitivityanalysis of regional air quality models. J. Comput. Phys., 204(1), 222–252, 2005.

Scheuer, E., Talbot, R. W., Dibb, J. E., Seid, G. K., deBell, L., and Lefer, G.: Seasonal distributions of fine aerosol sulfate in the North American Arctic Basin during TOPSE, J. Geophys. Res., 108, 8370, doi:doi:10.1029/2001JD001364, 2003.

Sillman, S.: The use of NO_y, H_2O_2, and HNO_3 as indicators for

ozone-NO_x-hydrocarbon sensitivity in urban locations, J. Geophys. Res., 100, 14175–14188, 1995.

Slusher, D. L., Huey, L. G., Tanner, D. J., Flocke, F. M., and Roberts, J. M.: A thermal dissociation-chemical ionization massspectrometry (TD-CIMS) technique for the simultaneous measurementof peroxyacyl nitrates and dinitrogenpentoxide, J. Geophys. Res., 109, D19315, doi:10.1029/2004JD004670, 2004.

Tang, Y., Carmichael, G. R., Horowitz, L. W., Uno, I., Woo, J.-H., Streets, D. G., Dabdub, D., Kurata, G., Sandu, A., Allan, J., Atlas, E., Flocke, F., Huey, L. G., Jakoubek, R. O., Millet, D. B., Quinn, P. K., Roberts, J. M., Worsnop, D. R., Goldstein, A., Donnelly, S., Schauffler, S., Stroud, V., Johnson, K., Avery, M. A., Singh, H. B., and Apel, E. C.: Multiscale simulations of tropospheric chemistry in the eastern Pacific and on the U.S. West Coast during spring 2002, J. Geophys. Res., 109, D23S11, doi:10.1029/2004JD004513, 2004.

Viswanathan, S., Eria, L., Diunugala, N., Johnson, J., and McClean, C.: An analysis of effects of San Diego wildfire on ambient air quality, J. Air Waste Manage. Assoc., 56(1), 56–67, 2006.

Vutukuru, S. and Dabdub, D.: Modeling the effects of ship emissions on coastal air quality: A case study of southern California, Atmos. Environ., 42, 3751–3764, 2008.

Wang, H., Jacob, D. J., Sager, P. L., Streets, D. G., Park, R. J., and Gilliland, A. B., and van Donkelaar, A.: Surface ozone background in the United States: Canadianand Mexican pollution influences. Atmos. Environ., 43, 1310–1319, 2009.

Weinheimer, A. J., Walega, J. G., Ridley, B. A., Gary, B. L., Blake,D. R., Blake, N. J., Rowland, F. S., Sachse, G. W., Anderson, B. E., and Collins, J. E.: Meridional distributions of NO_x, NO_y, and other species in the lower stratosphere and upper tropoSphereduring AASE II, Geophys. Res. Lett., 21, 2583–2586, 1994.

WRF/Chem Version 3.1 User's Guide: http://ruc.noaa.gov/wrf/WG11/Users_guide.pdf, 2009.